

Cruise ship's vibration behavior: simulation-measurement correlation analysis

Auteur : Salazar Loor, Lissette Priscilla

Promoteur(s) : 14958

Faculté : Faculté des Sciences appliquées

Diplôme : Master : ingénieur civil mécanicien, à finalité spécialisée en "Advanced Ship Design"

Année académique : 2020-2021

URI/URL : <http://hdl.handle.net/2268.2/13641>

Avertissement à l'attention des usagers :

Tous les documents placés en accès ouvert sur le site le site MatheO sont protégés par le droit d'auteur. Conformément aux principes énoncés par la "Budapest Open Access Initiative"(BOAI, 2002), l'utilisateur du site peut lire, télécharger, copier, transmettre, imprimer, chercher ou faire un lien vers le texte intégral de ces documents, les disséquer pour les indexer, s'en servir de données pour un logiciel, ou s'en servir à toute autre fin légale (ou prévue par la réglementation relative au droit d'auteur). Toute utilisation du document à des fins commerciales est strictement interdite.

Par ailleurs, l'utilisateur s'engage à respecter les droits moraux de l'auteur, principalement le droit à l'intégrité de l'oeuvre et le droit de paternité et ce dans toute utilisation que l'utilisateur entreprend. Ainsi, à titre d'exemple, lorsqu'il reproduira un document par extrait ou dans son intégralité, l'utilisateur citera de manière complète les sources telles que mentionnées ci-dessus. Toute utilisation non explicitement autorisée ci-avant (telle que par exemple, la modification du document ou son résumé) nécessite l'autorisation préalable et expresse des auteurs ou de leurs ayants droit.



POLITÉCNICA



Universität
Rostock



Traditio et Innovatio



SOLENT
UNIVERSITY
SOUTHAMPTON



Zachodniopomorski
Uniwersytet
Technologiczny
w Szczecinie



With the support of the
Erasmus+ Programme
of the European Union

CHANTIERS
DE L'ATLANTIQUE

Cruise ship's vibration behaviour: simulation-measurement correlation analysis

submitted on 07 September 2021

by

SALAZAR LOOR Lissette Priscilla

37 rue du Champ de Manoeuvres | 44470 Carquefou

lpsalazar@student.uliege.be

Student ID No.: S193098

Supervisor:

Hervé Le Sourne

ICAM

Reviewer:

Jonathan Ridley

Solent University



TABLE OF CONTENT

1. INTRODUCTION.....	6
2. DESCRIPTION OF THE STRUCTURES	7
2.1. General overview of the cruise ship	7
2.2. Deck 14 structure.....	8
2.3. Deck 15 structure.....	9
2.4. Cabin “RAMSESS”.....	11
2.5. Cabin model.....	11
3. MODAL RESPONSE	13
3.1. Theoretical background	13
3.2. Ansys Classic.....	15
3.3. Ansys Workbench.....	17
3.4. Results	21
3.4.1. Deck 14	21
3.4.2. Deck 15	25
3.4.3. Cabin “RAMSESS”.....	27
3.4.4. Cabin model	28
4. HARMONIC ANALYSIS	30
4.1. Theoretical background	30
4.2. Results in cabin model.....	32
5. MEASUREMENTS	36
5.1. Measurement system description.....	36
5.2. Deck 14.....	36
5.3. Deck 15.....	38
5.4. Cabin “RAMSESS”.....	40
5.5. Cabin model.....	42

6. CORRELATION.....	44
6.1. Modal analysis in decks.....	44
6.2. Modal analysis in cabin “RAMSESS”	47
6.3. Harmonic analysis in cabin model.....	48
7. CONCLUSIONS AND PERSPECTIVE	51
8. REFERENCES.....	53

Declaration of Authorship

I declare that this thesis and the work presented in it are my own and have been generated by me as the result of my own original research.

Where I have consulted the published work of others, this is always clearly attributed.

Where I have quoted from the work of others, the source is always given. With the exception of such quotations, this thesis is entirely my own work.

I have acknowledged all main sources of help.

Where the thesis is based on work done by myself jointly with others, I have made clear exactly what was done by others and what I have contributed myself.

This thesis contains no material that has been submitted previously, in whole or in part, for the award of any other academic degree or diploma.

I cede copyright of the thesis in favour of the Université de Liège and Universidad Politécnica de Madrid.

Date:

Signature

ABSTRACT

This work presents the analyses of different structures of a cruise ship to find the correlation between the vibrational behaviour performed by finite element method simulations and measurements on-site. The structures include deck areas in the ship under construction and real scale models of passengers' cabins. For the decks' areas, there is a comparison of two different applications of the finite element method in Ansys: Classic and Workbench.

A modal analysis was performed on two decks' sections in the area where passenger cabins will be installed. The differences between Ansys Classic and Workbench go from less than 1% to up to 20% depending on the closeness of the mesh size. Not all the mode shapes were easy to identify and not all of them visually match; the main differences between the models could be due to the different types of elements used to represent the structure's behaviour and the distribution of those elements over the decks' model. In the correlation with measurements from the test, there is not a clear tendency neither for Ansys Classic nor for Ansys Workbench to better fit with the measurements results, however, both show good results in terms of range of frequency. Some parameters could be influencing the resultant frequencies and have not been considered in the models.

Then, the modal analysis of a prototype of a passenger's cabin "Ramsess" is performed. At the time of the test, only the steel structure of the cabin was built, then, the model was formed by girders and pillars. The results of this analysis show a good correlation between the finite element model and the measurements, the maximum difference between the natural frequencies is 5%, and the mode shapes were easy to identify. It was possible to test two different support conditions to check the one which better represents the real structure, it was found that it depends on the main direction of the deformation.

Finally, the vibrational response of a cabin model is estimated by applying an external random excitation and compared with the finite element simulation. The model for finite element analysis was developed with a medium level of details, including the main steel structure, but excluding some non-structural parts. The results were compared in three points of the cabin's balcony showing a good correlation in magnitude and a maximum difference in the peak's frequencies of 16% for one of the points. In the other two points, the results do not correlate quite well probably due to an inaccurate representation of the model, not only by exclusion of some elements but also for the support condition.

1. INTRODUCTION

Knowing the vibrational behaviour of a ship is one of the key points to assure comfort onboard, for high-standard cruise vessels like the ones built by Chantiers de l'Atlantique, then, this point is carefully considered. The company analyses global and some local vibrations on the design stage and later performs measurements onboard especially on the passenger's cabin areas as well as on prototypes of the cabins before the installation.

The analysis of a complex structure as a passenger ship's deck would not be accurate by using analytical approximation formulas since it includes stiffened panels that could be non-regular arranged, pillars, bulkheads, and distributed masses. Moreover, local ship structures present comparatively high natural frequencies, and a proper definition of edges' conditions is a challenge.

As consequence, the structures must be reproduced in a finite element model with high precision to properly simulate the stiffening effect of all the elements. In addition, to achieve a more accurate condition for the boundaries of the studied area, the model should include a considerable part of its surroundings which will increase the modelling and solving difficulty and time.

Chantiers de l'Atlantique has developed a simplified and quick procedure with Excel files to create the deck's model and solve the modal analysis in Ansys Classic. The first objective is to compare the modal analysis results from this simplified procedure with a model in Ansys Workbench. Then, validate the use of the tool by comparing those results with the measurements made on the ship and analyse possible sources of the difference in results.

Since the company also built real scale prototypes of the cabins to check the acoustic behaviour before their inclusion in the design, the second objective is to compare the results from real scale models measurements with a modal and harmonic analysis performed using the finite element model and check if a simple model of the cabins is a good representation of the reality, or a highly detailed model should be prepared which would be time-consuming.

2. DESCRIPTION OF THE STRUCTURES

2.1. General overview of the cruise ship

The name of the ship studied is still confidential and it's known as M34. It is part of the Celebrity Edge Series luxury cruises built by Chantiers de L'Atlantique for the Royal Caribbean Cruises Ltd., Figure 2.1



Figure 2.1. Celebrity Edge cruise ship

The main characteristics are described in Table 2.1.

Table 2.1. Main characteristics of the cruise ship M34

Length overall	326 m
Max. breadth	39 m
Draught	8.2 m
Gross Registered Tonnage	140,000
Max. speed	22.6 kts
Passenger cabins	1,635
Passengers	3,937
Crew	1,416
Total propulsive power	32 MW
Flag	Malta
Classification	DNV
Construction material	Structural steel: Density = 7850 kg/m ³ Young modulus = 2.06e11 Pa Poisson's ratio = 0.3

For this study, the forward and starboard parts of deck 14 and deck 15 are modeled from frame 241 to 259 as marked in Figure 2.2.

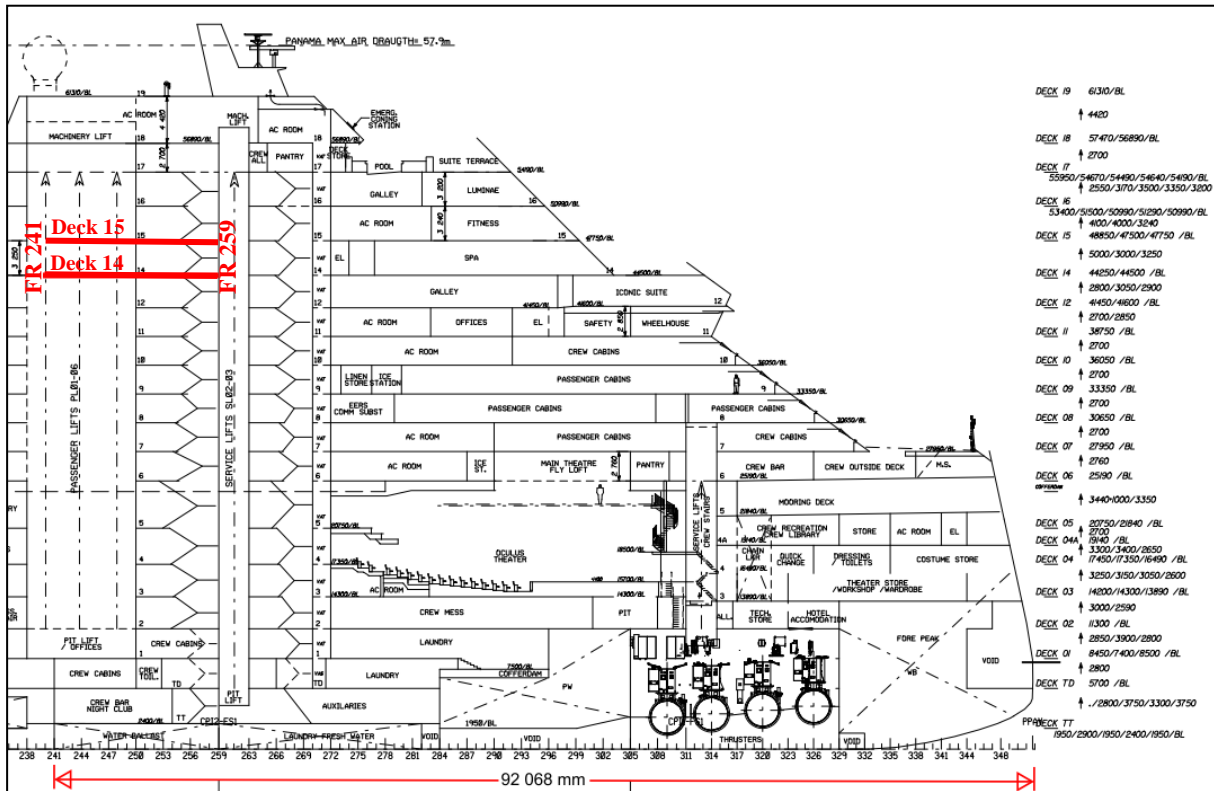


Figure 2.2. General distribution of M34 cruise ship, drawing from Chantiers de L'Atlantique.

2.2. Deck 14 structure

The structural distribution of the modeled part is composed of the following elements:

1. Deck plate, thickness = 7 mm
2. Longitudinal elements, reference center line at $y=0$, starboard side at $y=18.0$ m.
 - a. Girder, L 912 x 16, 250 x 15 mm, at $y=18.000$ m
 - b. Girder, T 780 x 10, 160 x 10 mm, at $y=15.335$ m
 - c. Girder, T 485 x 10, 200 x 10 mm, at $y=13.415$ m
 - d. Girder, T 485 x 10, 200 x 10 mm, at $y=7.985$ m
 - e. Girder, T 485 x 10, 200 x 10 mm, at $y=1.665$ m
 - f. 24 stiffeners, bulb flat 100 x 6 mm
3. Transversal elements, frame 241 at $x=224.54$ m, and frame 259 at $x=240.01$ m.
 - a. 05 Girders, T 485 x 7, 200 x 10 mm
4. Bulkheads
 - a. 06 longitudinal bulkheads over the deck, thickness = 6 mm, heigh = 3.25 m
 - b. 04 longitudinal bulkheads under the deck, thickness = 6 mm, heigh = 3.05 m

- c. 11 transversal bulkheads over the deck, thickness = 6 mm, heigh = 3.25 m
 - d. 06 transversal bulkheads under the deck, thickness = 6 mm, heigh = 3.05 m
 - e. Bulkheads' stiffeners bulb flat 100 x 6 mm
5. Pillars
- a. 07 square pillars over deck 120 x 120 mm, t=10 mm
 - b. 05 square pillars under deck 120 x 120 mm, t=10 mm
 - c. 03 round pillars under deck $\phi=139.7$ mm, t=10 mm
6. Surface mass
- a. 30 kg/m² overall deck surface
 - b. 150 kg/m² in addition over the Air Conditioning Room (ACR) surface

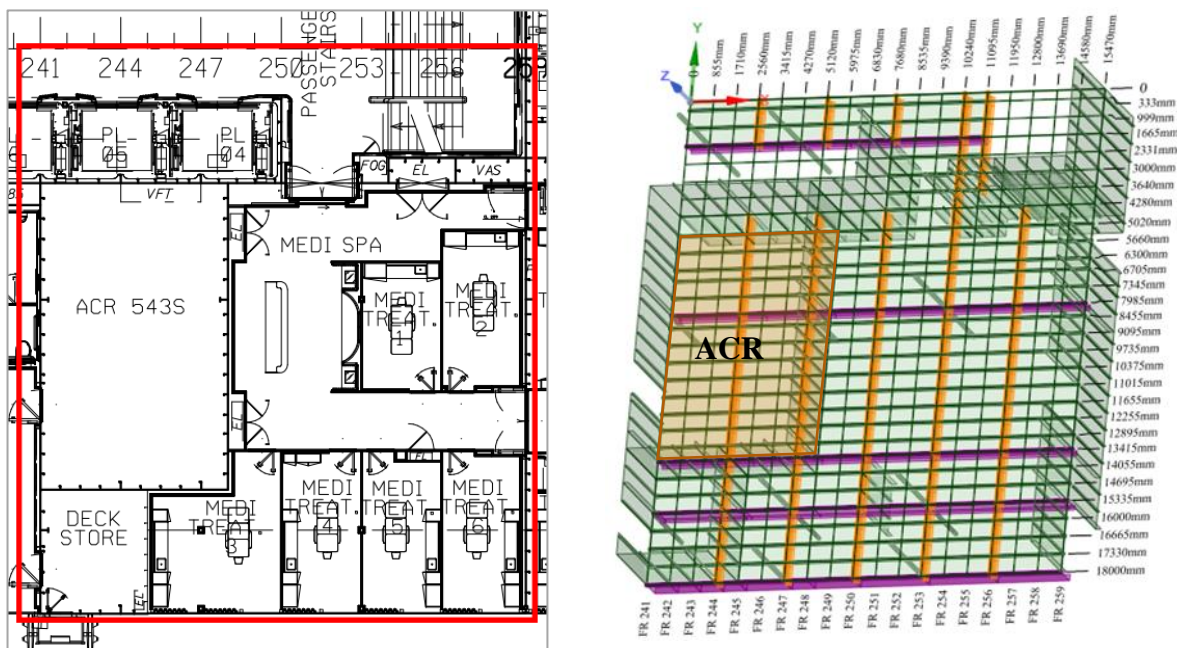


Figure 2.3. Modelled area of deck 14

2.3. Deck 15 structure

The structural distribution of the modeled part is composed of the following elements:

1. Deck plate, thickness = 5 mm
2. Longitudinal elements, reference center line at $y=0$, starboard side at $y=18.0$ m
 - a. Girder, L 880 x 10, 160 x 10 mm, at $y=18.000$ m
 - b. Girder, T 485 x 10, 200 x 10 mm, at $y=16.000$ m
 - c. Girder, T 485 x 10, 200 x 10 mm, at $y=15.335$ m
 - d. Girder, T 485 x 10, 200 x 10 mm, at $y=13.535$ m
 - e. Girder, T 485 x 10, 200 x 10 mm, at $y=9.095$ m

- f. Girder, T 485 x 10, 200 x 10 mm, at y=7.985 m
 - g. Girder, T 485 x 10, 200 x 10 mm, at y=1.665 m
 - h. 23 stiffeners, bulb flat 100 x 6 mm
3. Transversal elements, frame 241 at x=224.54 m, and frame 259 at x=240.01 m.
 - a. 05 girders, T 485 x 7, 200 x 10 mm
 - b. 01 girder, T 250 x 7, 160 x 10 mm at frame 254
4. Bulkheads
 - a. 06 longitudinal bulkheads over the deck, thickness = 6 mm, heigh = 3.24 m
 - b. 06 longitudinal bulkheads under the deck, thickness = 6 mm, heigh = 3.25 m
 - c. 09 transversal bulkheads over the deck, thickness = 6 mm, heigh = 3.24 m
 - d. 11 transversal bulkheads under the deck, thickness = 6 mm, heigh = 3.25 m
 - e. Bulkheads' stiffeners bulb flat 100 x 6 mm
5. Pillars
 - a. 06 square pillars over deck 120 x 120 mm, t=10 mm
 - b. 06 square pillars under deck 120 x 120 mm, t=10 mm
6. Surface mass
 - a. 30 kg/m² overall deck surface
 - b. Additional 39.3 kg/m² at cabin areas when floating floor is analyzed

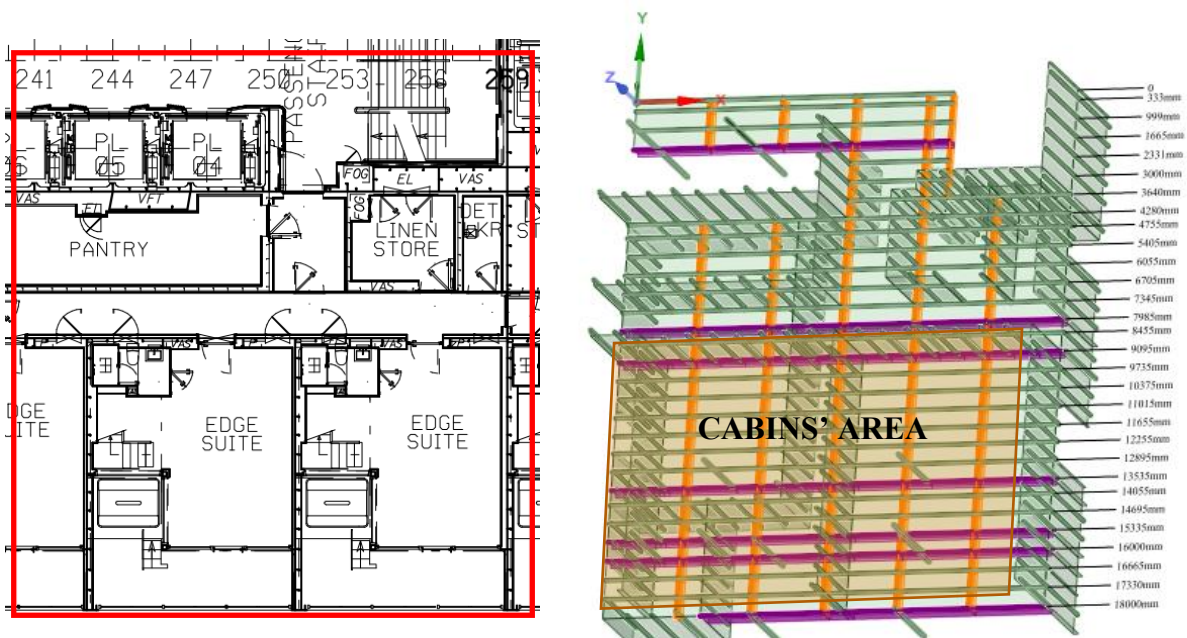


Figure 2.4. Modeled area of deck 15

2.4.Cabin “RAMSESS”

The structure is a prototype of a new passenger’s cabin that has been tested for future ship projects. It is composed of the following structural elements:

1. Elements in the x-direction
 - a. 02 girders, T 207 x 7, 100 x 10 mm
 - b. 04 stiffeners, I 84 x 5, 100 x 8 mm
2. Elements in the y-direction
 - a. 02 square pillars, 180 x 10 mm
 - b. 02 square pillars, 80 x 6 mm
3. Elements in the z-direction
 - a. 04 girders, I 207 x 7, 300 x 8, 80 x 8 mm



Figure 2.5. Structure of cabin model “Ramsess”

2.5.Cabin model

The structure is a prototype of a passenger’s cabin that will be installed in the cruise ship. It is composed of the following structural elements:

1. Upper and lower deck, thickness = 5 mm. An extra 5 mm plate was welded to the lower deck excluding the balcony area. In the model, this extra plate is represented as a distributed mass.
2. Side plates, thickness = 5 mm
3. Longitudinal elements, x-direction.
 - a. 02 girders, T 420 x 7, 160 x 10 mm
 - b. 10 stiffeners, T 100 x 6, 23 x 9 mm

4. Transversal elements, y-direction.
 - a. 03 girders in the upper deck, T 420 x 7, 160 x 10 mm, at $y=-2.596$ m, $y=0$ m, and $y=2.596$ m
 - b. 03 girders in the lower deck, T 420 x 7, 160 x 10 mm, at $y=-2.596$ m, $y=0$ m, and $y=2.596$ m
 - c. 04 stiffeners in the upper deck, flat plate 70 x 6 mm
 - d. 04 stiffeners in the lower deck, flat plate 70 x 6 mm
 - e. 04 stiffeners in each of both sides, flat plate 102.5 x 5 mm
5. Pillars
 - a. 03 square pillars in the cabin front part 160 x 160 mm, $t=10$ mm
 - b. 03 square pillars in the cabin back part 160 x 160 mm, $t=10$ mm
6. Additional mass
 - a. 39.4 kg/m² insulation in the upper deck
 - b. 2.0 kg/m² carpet in the lower deck
 - c. 39.3 kg/m² steel plate in the lower deck
 - d. 988 kg of a bell weight in the upper deck

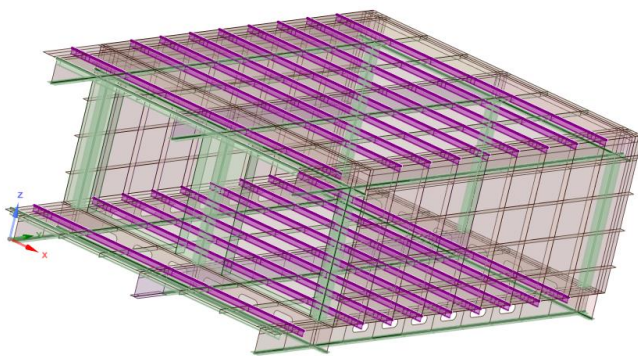


Figure 2.6. Structure distribution of cabin model

3. MODAL RESPONSE

3.1. Theoretical background

The modal response shows the vibration characteristics own of a structure, is the shape and the corresponding natural frequencies at which those shapes appear. A point to consider is that in modal analysis there are no external loads applied and we could say there is a free vibration of the structure. Eq. 3.1 describes the free vibration of a conservative system around an equilibrium position (Gérardin & J.Rixen, 2015). It is important to remark that in this analysis the structure is considered as linear elastic and, as consequence, the mass (M) and stiffness (K) are constant over time.

$$Kq(t) + M\ddot{q}(t) = 0 \quad \text{Eq. 3.1}$$

Where $q(t)$ is the displacement, and $\ddot{q}(t)$ the acceleration.

In this approach, the damping component has not been considered, as explained in (Gérardin & J.Rixen, 2015) Chapter 3, the damping term complicates considerably the solution of the problem and under the light damping assumption, the inclusion of the term creates a complex solution where the imaginary part represents the eigenfrequency of each mode close to the eigenfrequency of the undamped system and the real part represents the complexity of the mode.

We are interested in a solution for Eq. 3.1 excluding the modes associated with nonzero frequencies, i.e., rigid-body modes are not considered since the structure has restrictions on the boundaries. The solution, as explained in (Gérardin & J.Rixen, 2015) chapter 2, leads to solving the eigenvalue problem (Eq. 3.2) with n linear and homogenous equations and n real and positives roots ω^2 . To each root ω^2 (eigenvalue) corresponds a real solution x (eigenmode), if ω^2 is a root of the algebraic equation Eq. 3.3.

$$(K - \omega^2 M)x = 0 \quad \text{Eq. 3.2}$$

$$\det(K - \omega^2 M) = 0 \quad \text{Eq. 3.3}$$

The structure of the analysed area of decks 14 and 15 as well as the cabin model could be considered as a plate with stiffeners, we could expect a similar response of a rectangular plate (Leissa, 1969), with the nodal patterns shown in Figure 3.1. The structure of the cabin “Ramsess” could be considered as a structure formed by beams, then, we expect a beam shape

behavior, and the cabin model is a combination of different structures, we can expect different behaviours in different areas.

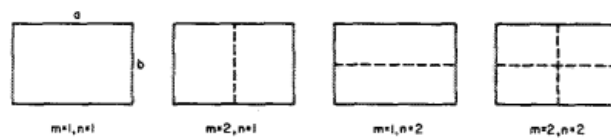


FIGURE 4.2.—Nodal patterns for SS rectangular plate with $a > b$.

Figure 3.1. Nodal patterns for SS rectangular plate, (Leissa, 1969)

The work of (Ferrari & Rizzuto, 2001) with a similar structure states that “*the modes that are present on the panel are categorized into two classes: those which show a significant displacement of stiffeners and those presenting mainly displacement in the plate (while stiffeners remain undeformed)*”. The results of this work in section 3.4 show a significant displacement of stiffeners.

Different authors have studied the free transverse vibrations of rectangular plates. (Warburton, 1954) approximated an expression to find the frequency for any combination of freely supported, free, and fixed edges and the corresponding modal shapes by using the Rayleigh method with deflection functions as the product of beam functions.

(Leissa, 1969) studied the frequency and nodal patterns of plates with different boundary conditions, shapes, among other variables, and correlated with experimental results. This work took as analytical base the work of (Warburton, 1954). However, those analyses were made in non-stiffened plates.

(Chen, Liu, & Chern, 1994) developed a spline compound strip method for the free vibration analysis of a stiffened plate. This method can be considered as an especial form of the finite element method owing to the plate being discretized in one direction. The presence of the stiffeners in the plate is represented by adding the stiffness and mass matrices of the stiffeners into the plate matrices at the element level and constraining the stiffener displacement field to the strip displacement fields.

In a complex structure as a cruise ship’s deck, the use of analytical approximation formulas would not be effective nor accurate, then, the structure must be reproduced in a finite element model. The finite element method consists of discretizing the structure in smaller elements of simple geometry with specific and identified structural characteristics, this process is known as meshing. The characteristics of the mesh along with material properties are used to

mathematically represent the stiffness and mass distribution of the structure, i.e., to generate stiffness and mass matrices.

Two applications of the same finite element software are used for deck 14 and deck 15, in both, plates are represented by shell elements, and girders, stiffeners, and pillars are represented by beam elements. The description of the application is oriented to the possible causes of differences in the results between Ansys Classic and Ansys Workbench. The results for the cabin model and “Ramsess” cabin are presented only in Ansys Workbench to be compared with measurements made in the prototypes.

3.2. Ansys Classic

The company Chantiers de L’Atlantique has developed a simplified method to generate the model on Ansys Classic from an Excel file and a group of macros where the structural distribution is described.

For deck 14 and deck 15, the mesh is automatically generated locating nodes on key points, the average distance between nodes in the x-direction is 900 mm and 500 mm in the y-direction. In z-direction, pillar’s beams elements are composed of two nodes, one in the deck surface and one in the pillar’s extreme.

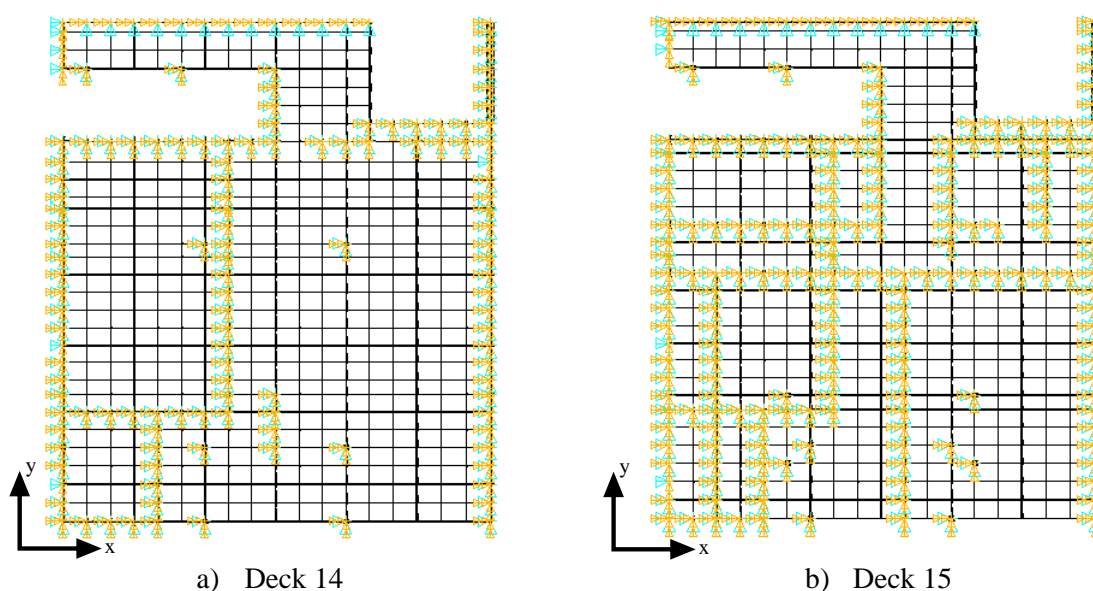


Figure 3.2. Mesh distribution in Ansys Classic

Two types of elements are included in the structure of the model for deck 14 and deck 15: Shell 63 for surfaces, and beam 44 for girders, stiffeners, and pillars. Cabins were not tested on Ansys Classic.

Shell 63 is a 3D linear quadrilateral element with four nodes and six degrees of freedom at each node as shown in Figure 3.3. The element stiffness considers bending and membrane effects and does not consider transverse shear deflection.

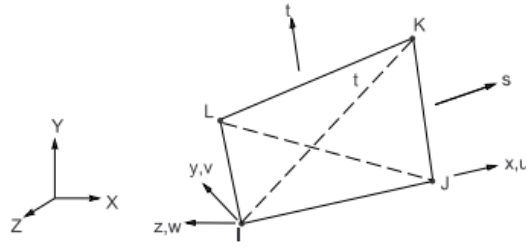


Figure 3.3. Geometry of element Shell 63

According to the Ansys Mechanical Theory Reference, the shape functions for this element correspond to the quadrilateral shells without shear deflection and with extra shape functions:

$$u = \frac{1}{4}(u_I(1-s)(1-t) + u_J(1+s)(1-t) + u_K(1+s)(1+t) + u_L(1-s)(1+t) + u_1(1-s^2) + u_2(1-t^2))$$

$$v = \frac{1}{4}(v_I(1-s) \dots (\text{analogous to } u))$$

$w = \text{not explicitly defined. Four overlaid triangles}$

Beam 44 is a 3D elastic tapered unsymmetric beam with 2 nodes and no internal integration points as shown in Figure 3.4; shear deflection effects are not included in the mass matrix.

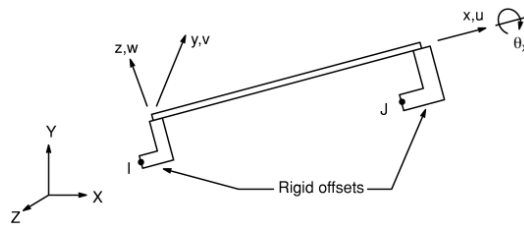


Figure 3.4. Geometry of element Beam 44

According to the Ansys Mechanical Theory Reference, the shape functions for this element correspond to the 2 node line elements, but excluding the shear deflection terms when the shape function is used to generate the mass matrix:

$$u = \frac{1}{2}(u_I(1-s)(1-t) + u_J(1+s))$$

$$v = \frac{1}{2} \left(v_I \left(1 - \frac{s}{2}(3-s^2) \right) + v_J \left(1 + \frac{s}{2}(3-s^2) \right) \right) + \frac{L}{8} (\theta_{z,I}(1-s^2)(1-s) - \theta_{z,J}(1-s^2)(1+s))$$

$$w = \frac{1}{2} \left(w_I \left(1 - \frac{s}{2} (3 - s^2) \right) + w_J \left(1 + \frac{s}{2} (3 - s^2) \right) \right) - \frac{L}{8} (\theta_{y,I} (1 - s^2) (1 - s) - \theta_{y,J} (1 - s^2) (1 + s))$$

$$\theta_x = \frac{1}{2} (\theta_{x,I} (1 - s) + \theta_{x,J} (1 + s))$$

The boundary conditions are defined in both decks as symmetry condition at centreline, frame 241 and frame 259, and free condition at the side. In addition, the pillars and bulkheads extremes are fixed as described in Table 3.1.

Table 3.1. Boundary conditions applied to Ansys Classic model

	Location	Boundary condition
Centreline	$y = 0$	$u_y = R_x = R_z = 0$
Frame 241	$x = 0$ (<i>local</i>) $x = 224.54$ m (<i>global</i>)	$u_x = R_y = R_z = 0$
Frame 259	$x = 15.47$ m (<i>local</i>) $x = 240.01$ m (<i>global</i>)	$u_x = R_y = R_z = 0$
Side	$y = 18.0$ m	free
Pillars extreme	Section 2.2 and 2.3	$u_x = u_x = u_z = R_x = R_y = R_z = 0$
Bulkheads		$u_x = u_x = u_z = R_x = R_y = R_z = 0$

The extraction method of the modes selected is Block Lanczos, which is widely used for large engineering projects in finite element software since it requires small computing effort compared with other extraction methods.

3.3. Ansys Workbench

The structures deck 14 and deck 15 were modeled in Space Claim by using surfaces for deck and bulkheads, and beams for girders, stiffeners, and pillars. The mesh is automatically generated for some different mesh sizes that were tested to approximate the average distance between nodes in Ansys Classic between 500 and 900 mm. Two types of elements are included in the structure of the model of deck 14 and deck 15: Shell 181 for surfaces, and beam 188 for girders, stiffeners, and pillars, Figure 3.5 a., and b.

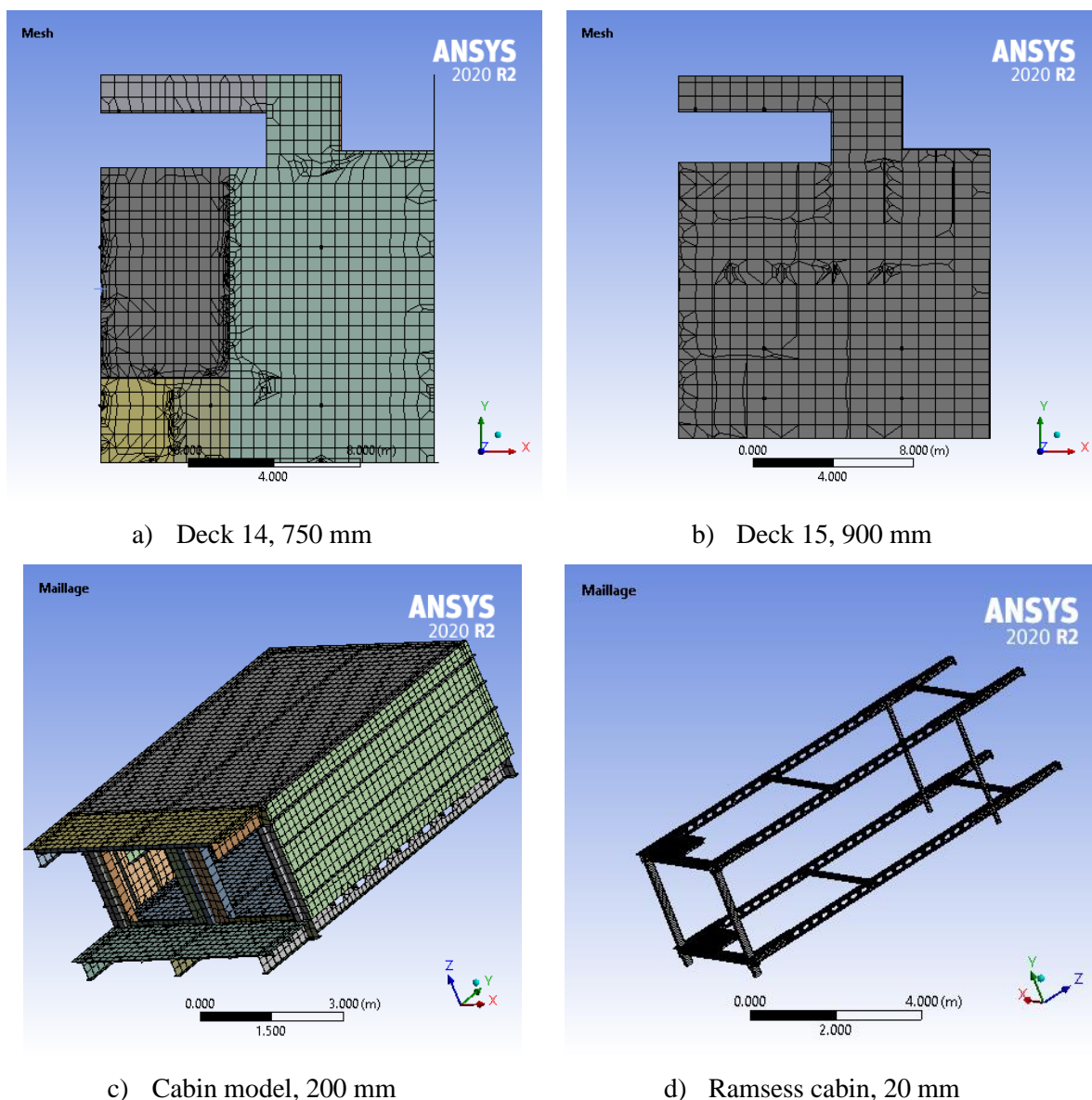


Figure 3.5. Mesh generated for each structure

For the cabin model, roof, floor, front, and side walls were modeled as shells, pillars as beams and for girders and stiffeners two types of models were tried: one with girders' webs and flanges as plates and the other one with webs as plates and flanges as beams as recommended by (Asmussen, Menzel, & Mumm, 2001) to check if there is any significant difference. The mesh was automatically generated with a size of 200 mm. For "Ramsess" cabin model, the small plates that are part of the structure are modeled as shells as well as the stiffeners and girders, and the pillars are modeled as beams. Figure 3.5 c. and d.

Shell 181 is a 3D linear quadrilateral element with four nodes and six degrees of freedom at each node. Includes the linear effects of transverse shear deformation. The through-thickness stress is zero.

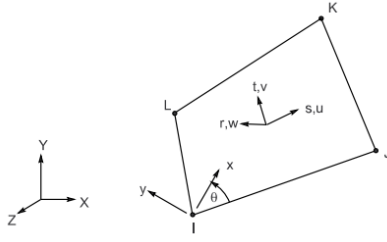


Figure 3.6. Geometry of element Shell 181

According to the Ansys Mechanical Theory Reference, the shape functions for this element correspond to the quadrilateral shell element, with shear deflection and without extra shape functions:

$$u = \frac{1}{4}(u_I(1-s)(1-t) + u_J(1+s)(1-t) + u_K(1+s)(1+t) + u_L(1-s)(1+t))$$

$$v = \frac{1}{4}(v_I(1-s) \dots (\textit{analogous to } u))$$

$$w = \frac{1}{4}(v_I(1-s) \dots (\textit{analogous to } u))$$

$$\theta_x = \frac{1}{4}(\theta_x(1-s) \dots (\textit{analogous to } u))$$

$$\theta_y = \frac{1}{4}(\theta_y(1-s) \dots (\textit{analogous to } u))$$

$$\theta_z = \frac{1}{4}(\theta_z(1-s) \dots (\textit{analogous to } u))$$

Beam 188 is a 3-D two-node beam, based on Timoshenko beam theory which is a first-order shear-deformation effects theory, (transverse shear strain remains constant, cross sections remain plane). The element allows the automatic use of internal nodes for additional degrees of freedom, the element's shape functions used in this work include the internal node marked as K in Figure 3.7.

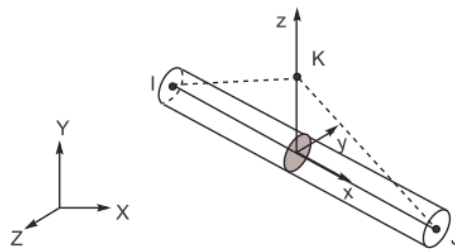


Figure 3.7. Geometry of element Beam 188

According to the Ansys Mechanical Theory Reference, the shape functions for this element correspond to the 3 node line elements:

$$u = \frac{1}{2} \left((u_I(-s + s^2) + u_J(s + s^2)) + u_k(1 - s^2) \right)$$

$$v = \frac{1}{2} \left((v_I(-s + s^2) + v_J(s + s^2)) + v_k(1 - s^2) \right)$$

$$w = \frac{1}{2} \left((w_I(-s + s^2) + w_J(s + s^2)) + w_k(1 - s^2) \right)$$

$$\theta_x = \frac{1}{2} \left((\theta_{x_I}(-s + s^2) + \theta_{x_J}(s + s^2)) + \theta_{x_k}(1 - s^2) \right)$$

$$\theta_y = \frac{1}{2} \left((\theta_{y_I}(-s + s^2) + \theta_{y_J}(s + s^2)) + \theta_{y_k}(1 - s^2) \right)$$

$$\theta_z = \frac{1}{2} \left((\theta_{z_I}(-s + s^2) + \theta_{z_J}(s + s^2)) + \theta_{z_k}(1 - s^2) \right)$$

The boundary conditions for deck 14 and deck 15 are the same as the ones applied for Ansys classic: symmetry condition at centreline, frame 241 and frame 259, and free condition at the side. In addition, the pillars and bulkheads extremes are fixed as described in Table 3.1.

For the cabin model and “Ramsess” cabin model simply supported and fixed conditions were tested in the areas marked in Figure 3.8. Like in Ansys classic, the extraction method of the modes is Block Lanczos.

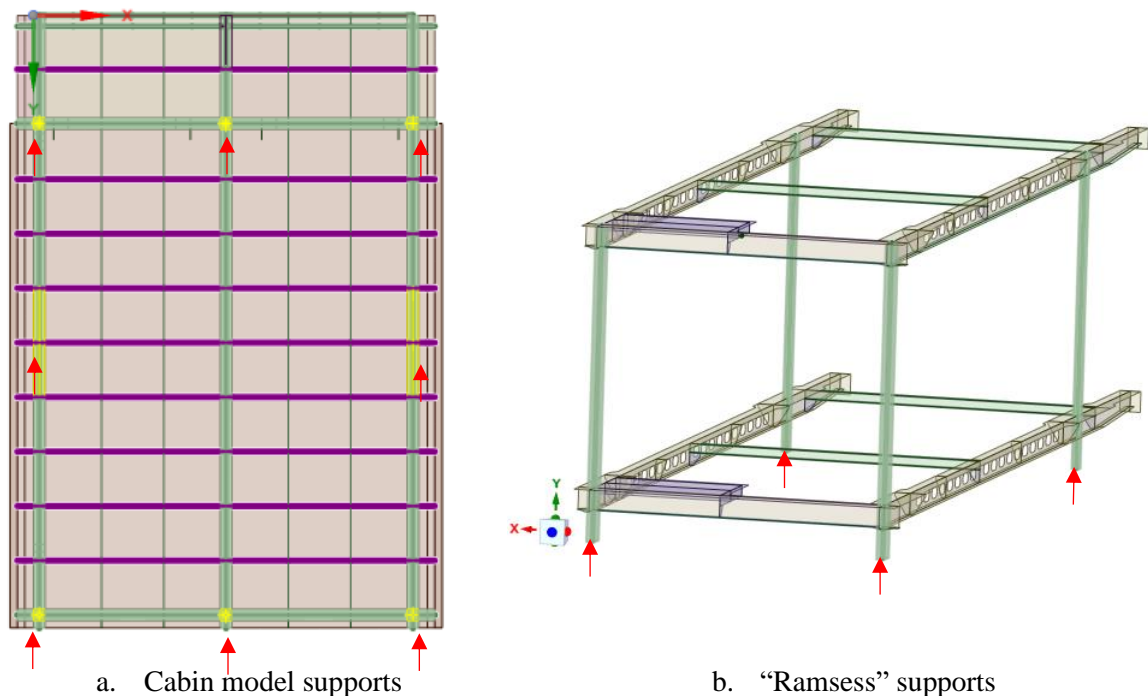


Figure 3.8. Support conditions for cabin model and Ramsess model

3.4. Results

3.4.1. Deck 14

Considering a frequency range between 1 and 50 Hz for the solution of the eigenvalue problem, different mesh sizes were tested in Ansys Workbench to decide the one that better represents the model to compare with Ansys Classic. The area selected for mesh comparison is the area where the measurements were done in the ship: between frames 250 and 256 in the x-direction and between 7.985 and 13.415 m in the y-direction, this comparison is shown in Table 3.2,

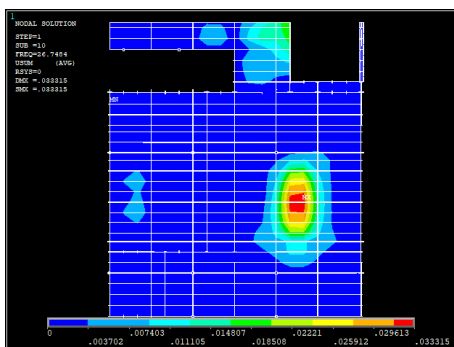
For this work, a good correlation means that the difference between results is less than 10%. The first two modes selected have close results and seem to be even closer when the mesh size is approaching 900 mm. The third mode does not present a good relation between Ansys Classic and Workbench for bigger mesh size; in an attempt of decreasing this difference, smaller meshes were tested but some “parasite” modes appeared in other zones of the deck increasing the number of modes to be extracted to get the mode shapes in the area of interest. This reduction in mesh increased considerably the computation time and didn’t present a significative change in the frequency results.

Table 3.2. Comparison of different mesh sizes for deck 14 on Ansys Workbench at measurement area

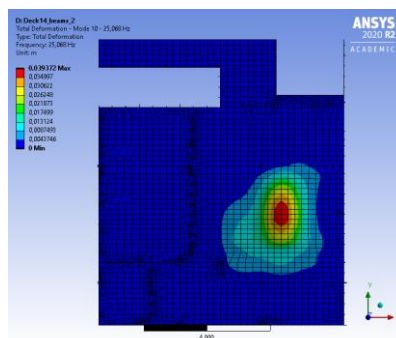
	First mode		Second mode		Third mode	
A. Classic	26.7 Hz		29.9 Hz		31.6 Hz	
Mesh size (m)	Hz	% Difference with A. Classic	Hz	% Difference with A. Classic	Hz	% Difference with A. Classic
0.50	25.1	6.3%	26.7	10.7%	33.7	6.6%
0.60	25.2	5.7%	27.0	9.8%	34.1	7.9%
0.75	26.0	2.8%	28.2	5.8%	37.6	19.1%
0.80	26.0	2.8%	28.2	5.8%	37.6	19.1%
0.90	26.7	0.03%	29.5	1.3%	40.6	28.6%

The modes at this area are found as a significant displacement of the stiffeners with the plate, taking the modal shape as a plate enclosed between transversal girders at frames 253 and 256 in the x-direction and longitudinal girders between 7.985 and 13.415 m in the y-direction. The shape deformation is shown in Figures 3.9, 3.10, and 3.11.

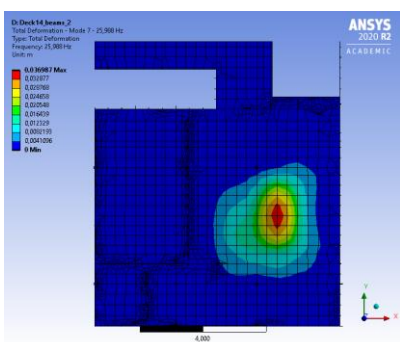
First mode in the measurement area



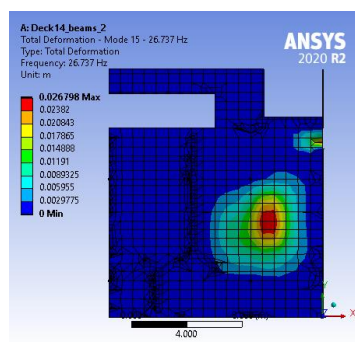
a) Ansys Classic, 26.7 Hz



b) Workbench, mesh 500mm, 25.1 Hz



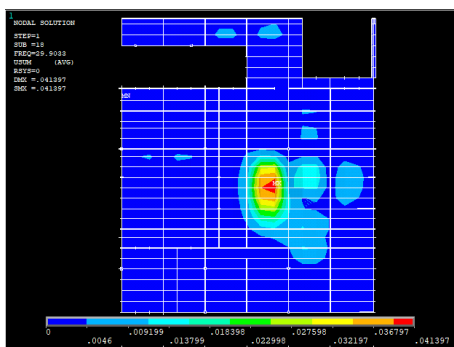
c) Workbench, mesh 750mm, 26.0 Hz



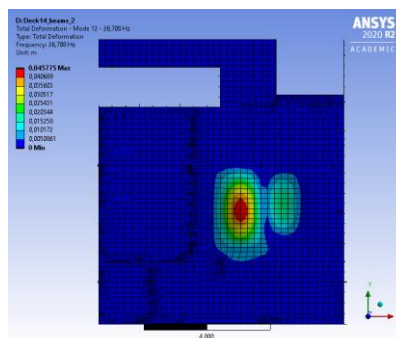
d) Workbench, mesh 900mm, 26.7 Hz

Figure 3.9. Deck 14, first mode results at measurement area in Ansys Classic and Workbench

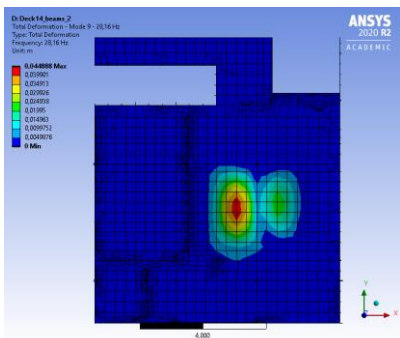
Second mode in measurement area



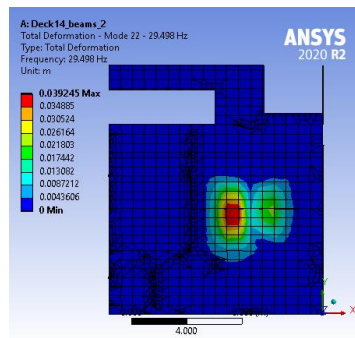
a) Ansys Classic, 29.9 Hz



b) Workbench, mesh 500 mm, 26.7 Hz



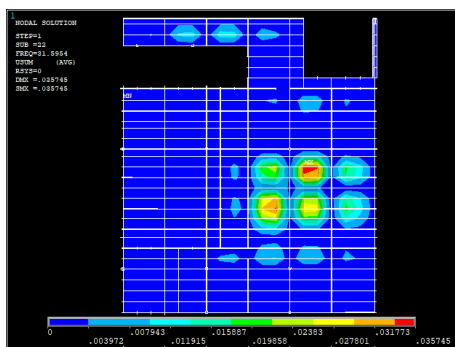
c) Workbench, mesh 750 mm, 28.2 Hz



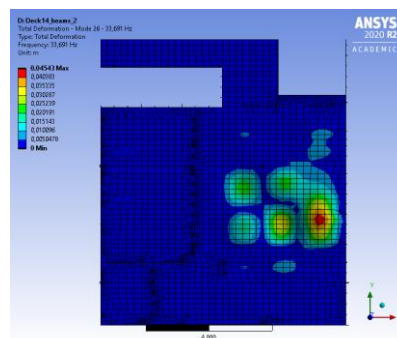
d) Workbench, mesh 900 mm, 29.5 Hz

Figure 3.10. Deck 14, second mode results at measurement area in Ansys Classic and Workbench

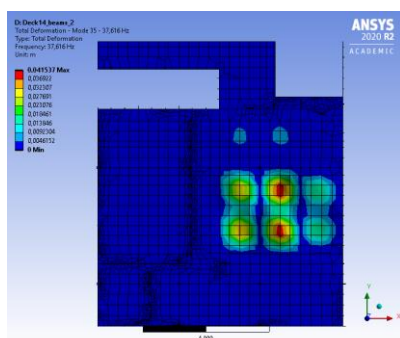
Third mode in measurement area



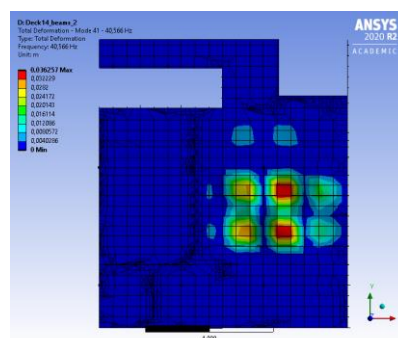
a) Ansys Classic, 31.6 Hz



b) Workbench, mesh 500mm, 33.7 Hz



c) Workbench, mesh 750mm, 37.6 Hz



d) Workbench, mesh 900mm, 40.6 Hz

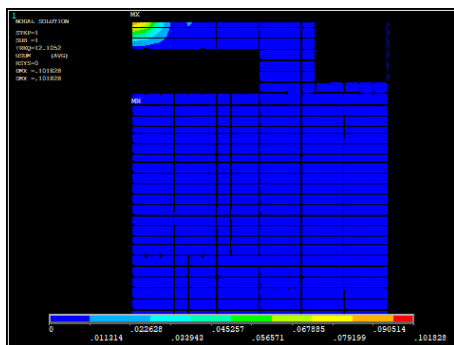
Figure 3.11. Deck 14, third mode results at measurement area in Ansys Classic and Workbench

Then, deformation shapes on the hallway and Air Conditioning Room (ACR) were also tested obtaining the results in Table 3.3 and shapes in Figures 3.12, 3.13, and 3.14. Modes in other areas that appear at higher frequency do not present a good relation in shape nor frequency between Ansys Classic and Ansys Workbench.

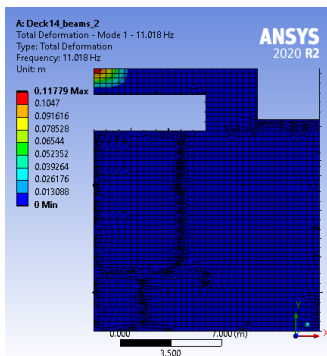
Table 3.3. Comparison of different mesh sizes for deck 14 on Ansys Workbench, hallway, and ACR

	Mode on hallway		First mode ACR		Second mode ACR	
A. Classic	12.1 Hz		20.4 Hz		24.9 Hz	
Mesh size (m)	Hz	% Difference with A. Classic	Hz	% Difference with A. Classic	Hz	% Difference with A. Classic
0.50	11.0	9.0%	20.0	1.9%	24.5	1.6%
0.75	11.4	6.0%	20.6	1.0%	27.0	8.5%
0.90	11.7	3.2%	22.9	12.2%	Not found	

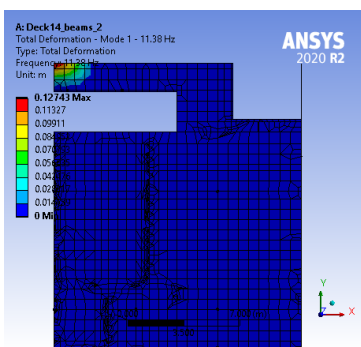
Mode on hallway



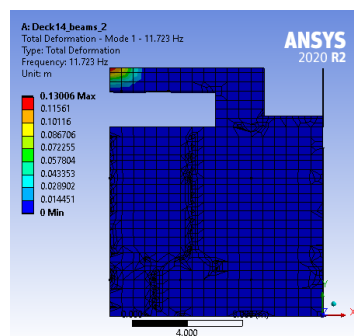
a) Ansys Classic, 12.3 Hz



b) Workbench, mesh 500mm, 11.0 Hz



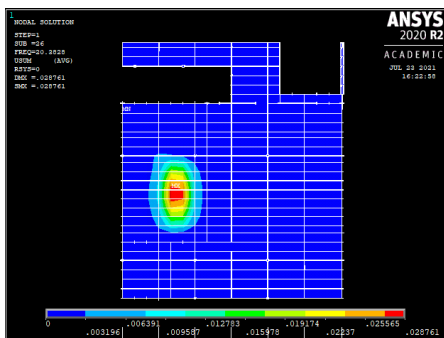
c) Workbench, mesh 750mm, 11.4 Hz



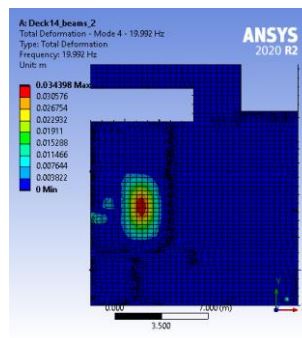
d) Workbench, mesh 900mm, 11.7 Hz

Figure 3.12. Deck 14, results at hallway area in Ansys Classic and Workbench

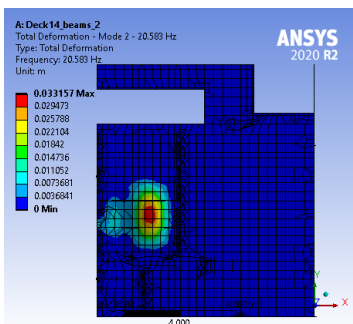
First mode on ACR



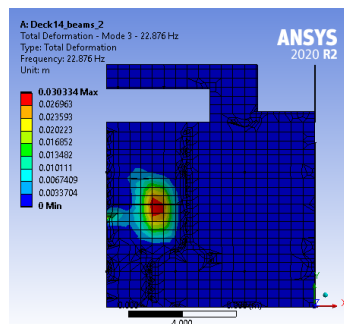
a) Ansys Classic, 20.4 Hz



b) Workbench, mesh 500 mm, 20.0 Hz



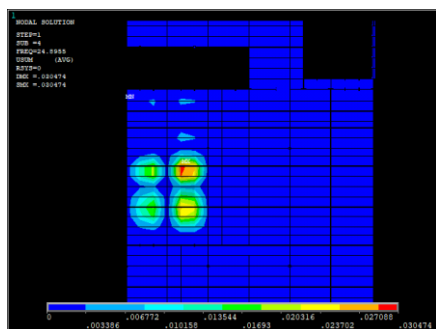
c) Workbench, mesh 750 mm, 20.6 Hz



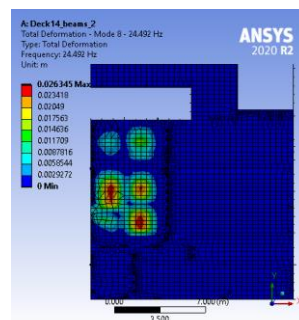
d) Workbench, mesh 900 mm, 22.9 Hz

Figure 3.13. Deck 14, first mode results at ACR area in Ansys Classic and Workbench

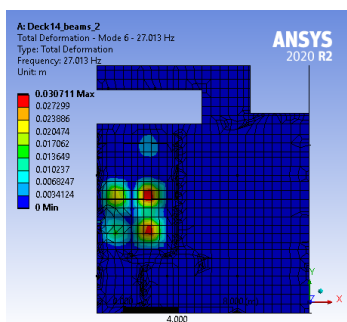
Second mode on ACR



a) Ansys Classic, 24.9 Hz



b) Workbench, mesh 500mm, 24.5 Hz



c) Workbench, mesh 750mm, 23.0 Hz

d) Workbench, mesh 900mm, -Hz

Not found

Figure 3.14. Deck 14, second mode results at ACR area in Ansys Classic and Workbench

3.4.2. Deck 15

Like deck 14, a frequency range between 1 and 50 Hz for the solution of the eigenvalue problem is considered, and different mesh sizes were tested in Ansys Workbench to decide the one that better represents the model to compare with Ansys Classic. The area selected for mesh comparison is the area where the measurements were done in the ship: between frames 250 and 256 in the x-direction and between 7.985 and 13.535 m in the y-direction. This comparison is shown in Table 3.4, for this structure, an additional analysis is presented including a floating floor with a surface mass of 39.4 kg/m^2 in the passengers' cabin area.

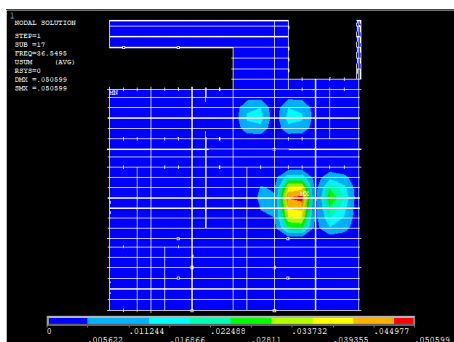
The modes at this area are also found as a significant displacement of the stiffeners with the plate, taking the modal shape as a plate enclosed between transversal girders at frames 253 and 256 in the x-direction and longitudinal girders between 9.095 and 13.535 m in the y-direction. The shape deformation is shown in Figure 3.15 and 3.16.

Table 3.4. Comparison of different mesh sizes for deck 15 on Ansys Workbench

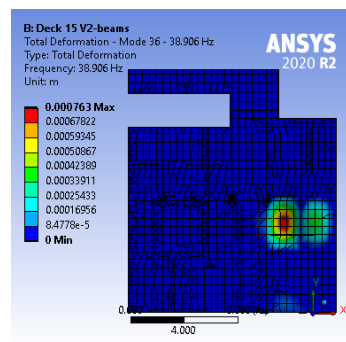
	Without floating floor				With floating floor			
	First mode		Second mode		First mode		Second mode	
A. Classic	36.5 Hz		38.2 Hz		29.9 Hz		31.2 Hz	
Mesh size (m)	Hz	% Difference with A. Classic	Hz	% Difference with A. Classic	Hz	% Difference with A. Classic	Hz	% Difference with A. Classic
0.25	33.2	9.2%	-	-	-	-	-	-
0.50	38.9	6.4%	49.6	30.1%	32.4	8.4%	41.4	32.8%
0.60	40.3	10.4%	51.7	35.4%	33.5	12.4%	43.5	39.7%
0.75	42.5	16.4%	52.7	38.1%	35.5	19.0%	45.5	45.9%
0.90	43.5	19.0%	53.2	39.5%	36.4	22.0%	46.5	49.1%

First mode in the measurement area

Without floating floor

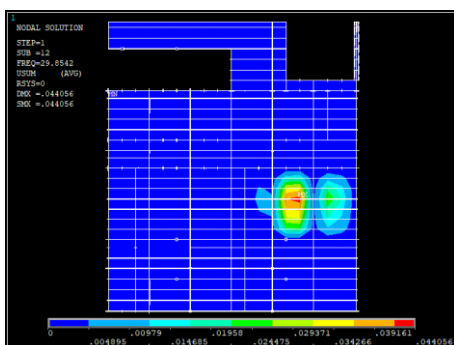


a) Ansys Classic, 36.55 Hz

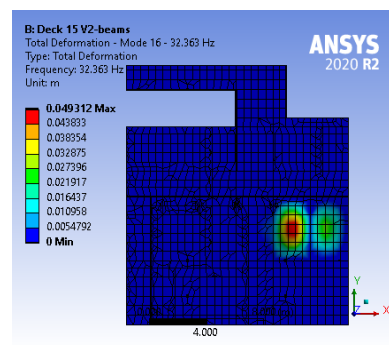


b) Workbench, mesh 500mm, 38.91 Hz

With floating floor



c) Ansys Classic, 29.85 Hz



d) Workbench, mesh 500mm, 32.36 Hz

Figure 3.15. Deck 15 with and without a floating floor, first mode in measurement area results

Second mode in the measurement area

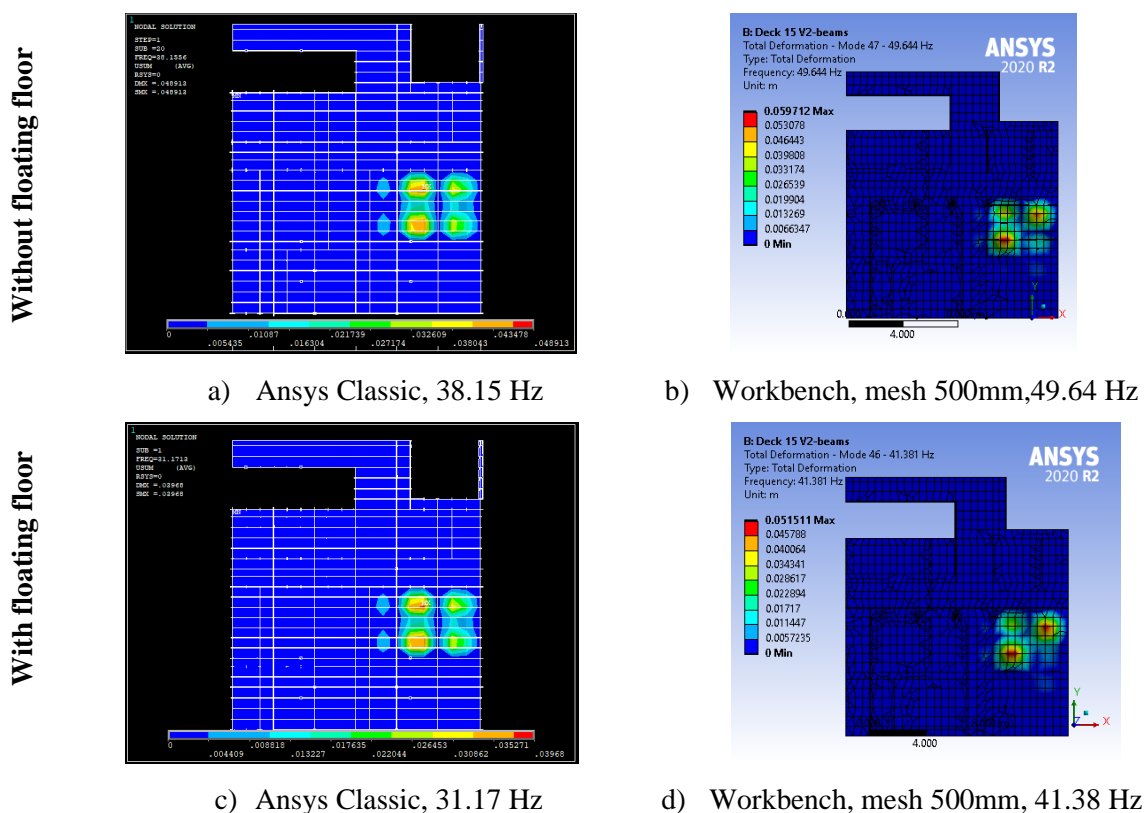


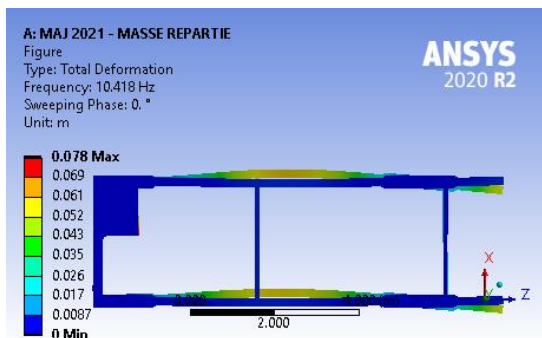
Figure 3.16. Deck 15 with and without a floating floor, second mode in measurement area results

It was not possible to find a consistent relation between the results in Ansys Classic and Ansys Workbench. Except for a few modes, the shapes are not coincident, and the differences increase for higher modes.

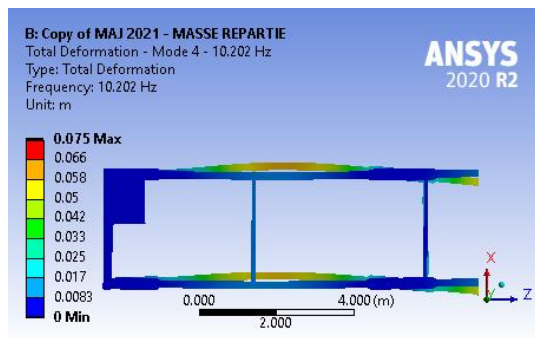
3.4.3. Cabin “RAMSESS”

The modal analysis for the “Ramsess” structure was made in Ansys Workbench and will be compared with measurements in the prototype. Therefore, the results presented here are the modes with high displacement mainly in the lower girders, where the test was made; two kinds of supports are tested to determine the one that better represents the real support by comparing with the measurements. A frequency range between 1 and 50 Hz for the solution of the eigenvalue problem is considered.

Mode 1

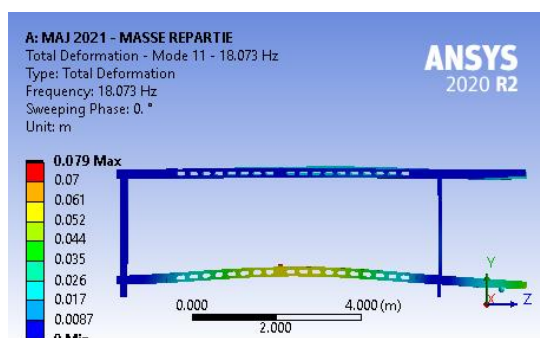


a) Supports fixed, 10.42 Hz

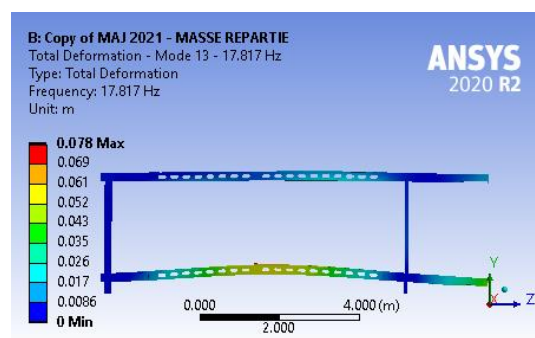


b) Simply supported, 10.20 Hz

Mode 2

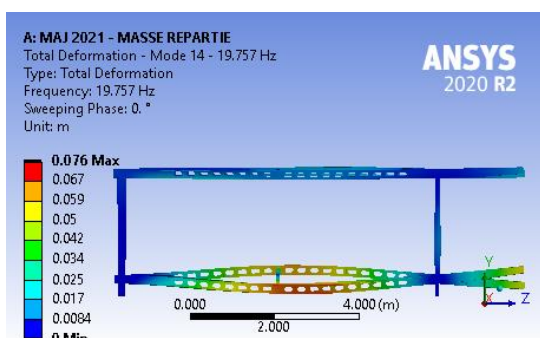


c) Supports fixed, 18.07 Hz

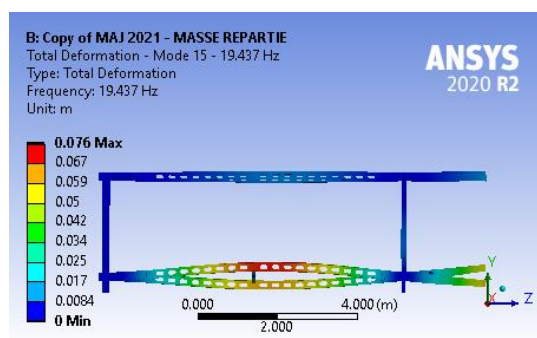


d) Simply supported, 17.82 Hz

Mode 3



e) Supports fixed, 19.76 Hz



f) Simply supported, 19.44 Hz

Figure 3.17. Ramsess cabin, mode results

3.4.4. Cabin model

The modal analysis for the cabin model structure was made in Ansys Workbench to be used later in the harmonic analysis and to be compared with harmonic response measurements made in the prototype. A frequency range between 1 and 150 Hz for the solution of the eigenvalue problem is considered. The modal density is presented in Table 3.5 and will be considered for the harmonic analysis, the frequency range values are 1/3 octave frequency band, as explained in section 4.1.

Table 3.5. Modal density cabin model

Frequency band		Modal density	Frequency band		Modal density
f_0	$1.26 f_0$		f_0	$1.26 f_0$	
10.00	12.60	0	40.02	50.42	81
12.60	15.88	1	50.42	63.53	26
15.88	20.00	6	63.53	80.05	79
20.00	25.20	11	80.05	100.86	117
25.20	31.76	6	100.86	127.08	143
31.76	40.02	36	127.08	160.12	107

Three modes' results are shown in Figure 3.18, including the one whose shape presents a high displacement amplitude in the measured points at the prototype: balcony (mode 3).

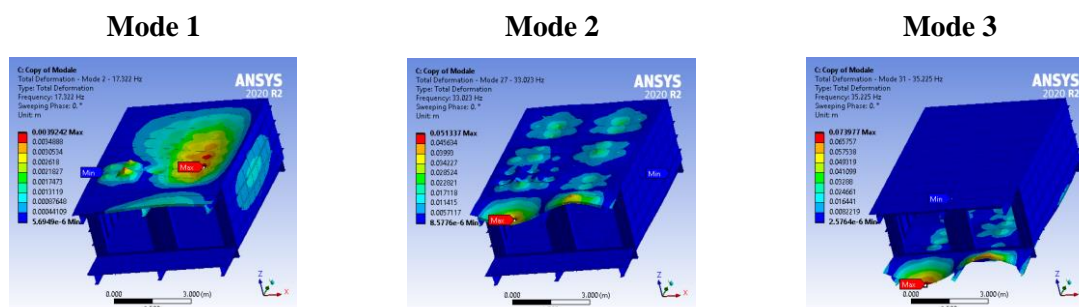


Figure 3.18. Results for three modes on the cabin model

The numerical analysis was made with different parameters to check their influence on the modal response of this structure. It was tested with a structural damping ratio of 2% and without damping; also, with two kinds of models for girders: one with girders' webs and flanges as plates and the other one with webs as plates and flanges as beams as recommended by (Asmussen, Menzel, & Mumm, 2001). Finally, simply supported, and fixed supports were tested. It is noticeable that those changes do not influence the mode frequency results as shown in Table 3.6.

Table 3.6. Comparison of damped/undamped and plates/beams for the cabin model

Mode	Damped	Difference	Plates	Difference	SS	Difference
	Undamped		Beam		Fixed	
1	17.322 Hz	0.006%	17.321 Hz	0.115%	17.341 Hz	0.352%
	17.321 Hz		17.341 Hz		17.402 Hz	
2	33.023 Hz	0.006%	33.021 Hz	0.124%	33.021 Hz	0.082%
	33.021 Hz		33.062 Hz		33.035 Hz	
3	35.225 Hz	0.006%	35.223 Hz	0.258%	35.223 Hz	0.547%
	35.223 Hz		35.132 Hz		35.324 Hz	

4. HARMONIC ANALYSIS

4.1. Theoretical background

The vibration response of the system to an imposed external harmonic excitation is important because a harmonic regime is representative of many possible cyclical loads in the structure of a ship, (engine, propeller, waves, etc). Eq. 4.1 describes the harmonic motion resulting from the application of a harmonic force of frequency ω (Géradin & J.Rixen, 2015). Like in the modal analysis, the structure is considered as linear elastic and, as consequence, the mass (M) and stiffness (K) are constant over time.

$$Kq(t) + C\dot{q}(t) + M\ddot{q}(t) = fe^{i\omega t} \quad \text{Eq. 4.1}$$

Where, $q(t)$, $\dot{q}(t)$ and $\ddot{q}(t)$ are the displacement, velocity, and acceleration fields respectively, ω is the excitation frequency and f describes the spatial distribution of the excitation amplitude.

Assuming that the response is limited to the forced term $q(t) = ze^{i\omega t}$, the solution as explained in (Géradin & J.Rixen, 2015) chapter 3, leads to solving the complex equation of Eq. 4.2.

$$(K - \omega^2 M + i\omega C)z = f \quad \text{Eq. 4.2}$$

One method to solve Eq. 4.2 is by the linear combination of mode shapes, or Mode Superposition Method (MSP). Assuming weak damping and decoupled equations, we can define a nondimensional damping ratio of a mode r Eq. 4.3, and the response amplitude in terms of n eigenmodes $x_{(s)}$ Eq. 4.4.

$$\varepsilon_r = \frac{\beta_r}{2\omega_{0r}\mu_r}; \quad \text{Eq. 4.3}$$

Where, β_r : *damping coefficient of mode r*

ω_{0r} : *eigenfrequency of mode r*

μ_r : *generalized mass of mode r , $\mu_r = x_{(r)}^T M x_{(r)}$*

$$z = \sum_{s=1}^n \alpha_s x_{(s)} \quad \text{Eq. 4.4}$$

The orthogonality relationships together with the modal damping assumption provide the coefficient for each of the eigenmodes $x_{(s)}$, Eq. 4.5.

$$\alpha_r = \frac{x_{(r)}^T f}{\mu_r (\omega_{0r}^2 - \omega^2 + 2i\varepsilon_r \omega \omega_{0r})} \quad \text{Eq. 4.5}$$

Combining the previous equations, we can obtain the spectral expansion of the dynamic influence coefficient matrix (admittance matrix) which depends on the frequency as described in Eq. 4.6.

$$(K - \omega^2 M + i\omega C)^{-1} = \sum_{s=1}^n \frac{1}{(\omega_{0s}^2 - \omega^2 + 2i\varepsilon_s \omega \omega_{0s})} \frac{x_{(s)} x_{(s)}^T}{\mu_s} \quad \text{Eq. 4.6}$$

However, the damping ratio ε_r (or modal damping) is not a pre-defined value and depends on the characteristics of each structure, it could be obtained by experimental measurements. If the results of experimental measurements are available, knowing the damping ratio for two eigenfrequencies would allow constructing the damping matrix \mathbf{C} of Eq. 4.2.

As we are assuming weak damping, we can define the matrix \mathbf{C} as a diagonal proportional damping matrix, Eq. 4.7 with damping coefficients in the form of Eq. 4.8.

$$\mathbf{C} = a\mathbf{K} + b\mathbf{M} \quad \text{Eq. 4.7}$$

$$\beta_r = a\gamma_r + b\mu_r \quad \text{Eq. 4.8}$$

Replacing Eq. 4.8. in Eq. 4.3 and with two known eigenfrequencies from experiments, the values of \mathbf{a} and \mathbf{b} can be found, Eq. 4.9.

$$\varepsilon_r = \frac{1}{2} \left(a\omega_{0r} + \frac{b}{\omega_{0r}} \right) \quad \text{Eq. 4.9}$$

It should be remarked that even if the mode superposition method achieved great acceptance for calculation of the forced vibration level. (Asmussen, Menzel, & Mumm, 2001), it is not appropriate for systems with high frequency and high modal density (Le Sourne, 2017).

Another procedure to solve the complex expression of Eq. 4.2 is through the direct method which uses the structural response of the system. The displacement vector $q(t)$ is found by directly solving a system of simultaneous equations for each excitation frequency using a static solver designed for complex arithmetic by expressing the motion equation as Eq. 4.10.

$$K_c q_c(t) = F_c(t) \quad \text{Eq. 4.10}$$

$$K_c = K - \omega^2 M + i\omega C \quad \text{Eq. 4.11}$$

$$q_c(t) = q_1(t) + iq_2(t) \quad \text{Eq. 4.12}$$

$$F_c(t) = F_1(t) + iF_2(t) \quad \text{Eq. 4.13}$$

ω : imposed circular frequency $\left(\frac{\text{radians}}{\text{time}}\right)$

$q_1(t)$: real displacement vector

$q_2(t)$: imaginary displacement vector

$F_1(t)$: real force vector

$F_2(t)$: imaginary force vector

This direct method is useful in a medium frequency domain, does not need the modes computation, and allows the exploration of higher frequencies. However, it is limited in frequencies by the element size, (Le Sourne, 2017) and generally is slower than MSP.

According to (Coppolino, 2010) the finite element is an effective approach for structures' dynamics if the vibration modes have a low modal density. Modal density is typically described as the number of modes within a 1/3 octave frequency band ($f_0 < f < 1.26f_0$) When the modal density of a structure is greater than 10 modes per 1/3 octave band, individual vibration modes are not of significance and the statistical energy analysis (SEA) method applies better.

4.2. Results in cabin model

The excitation force used for applying in the model to get the harmonic response is the same applied to the system by a generator (shaker) during the measurements. The spectrum of the force goes from 0 to 150 Hz.

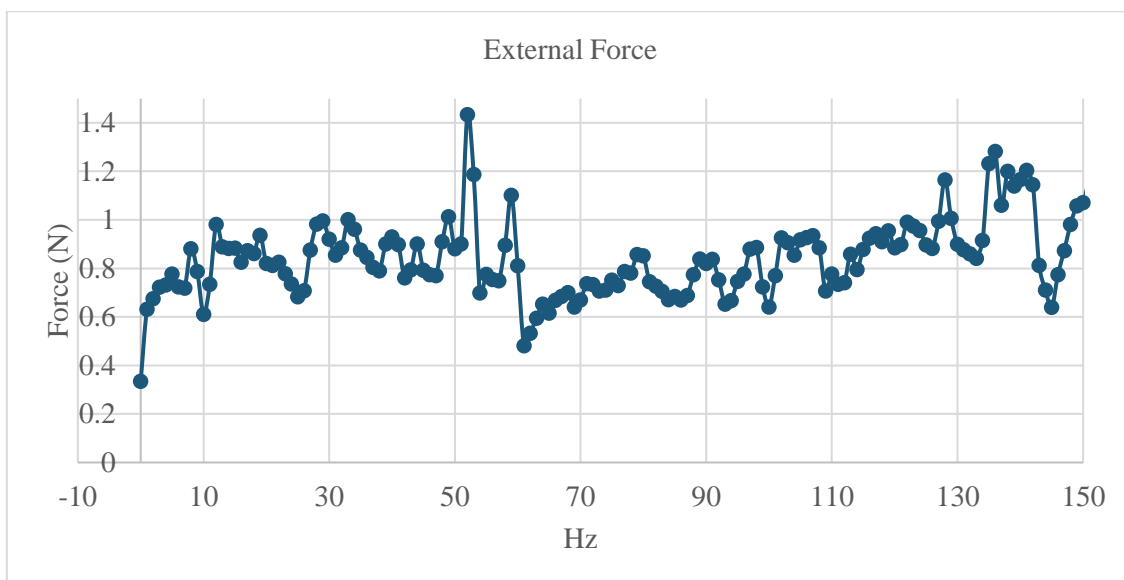


Figure 4.1. Excitation force applied to cabin model

The application point of the vertical force (z-direction) is on the central girder extreme, as shown with the red arrow in Figure 4.2 as well as the points selected for the presentation of results. The selection of these points is made based on the location of the accelerometers during measurements as will be explained in Section 5.5.

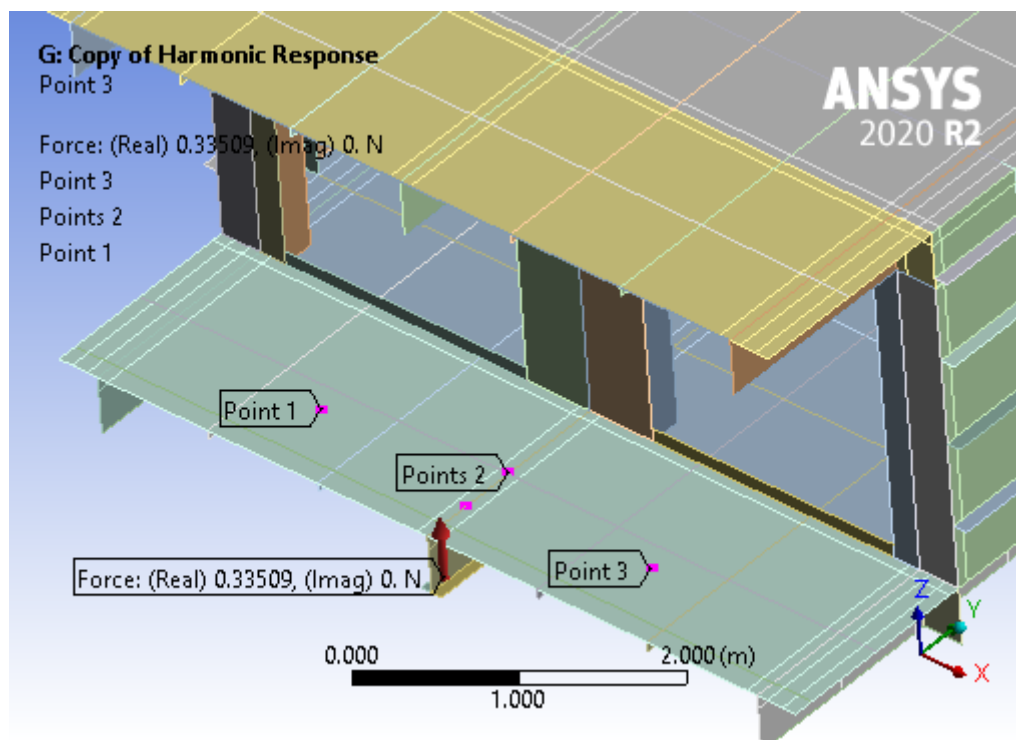


Figure 4.2. Points selected for the presentation of results on the model and force point

Results for each point are presented in a frequency range from 0 to 150 Hz and two methods were used for calculating the harmonic response: Mode superposition (MSP) and full method at the three selected areas. The “Full method” in Ansys is the direct solution method explained

in section 4.1. The results are presented in Figures 4.3, 4.4, and 4.5 and will be compared with the measurements results in section 5.5. A damping ratio coefficient of 2 % was imposed.

Points 1 and 3 present the highest peak at 150 Hz, as well as peaks at around 82, 46, and 32 Hz. On point 2 the highest peak appears at 117 Hz, there are smaller peaks at 82 and 46 Hz, this area presents a lower response than the other two points, it should be remarked that the accelerometers are located on the middle girder.

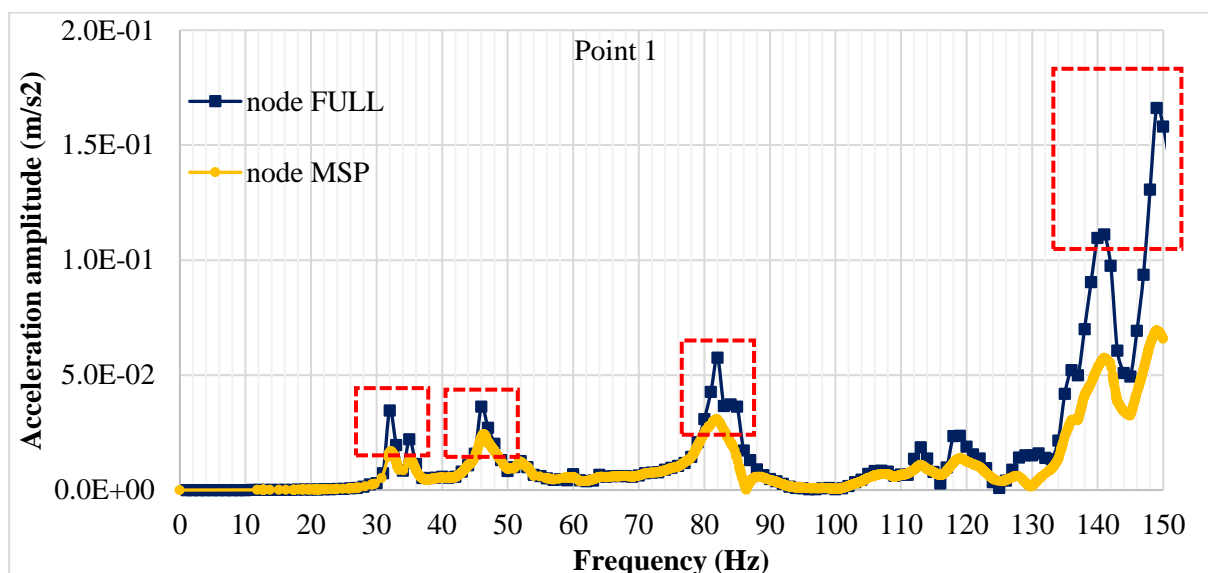


Figure 4.3. Harmonic response Ansys Workbench in Point 1

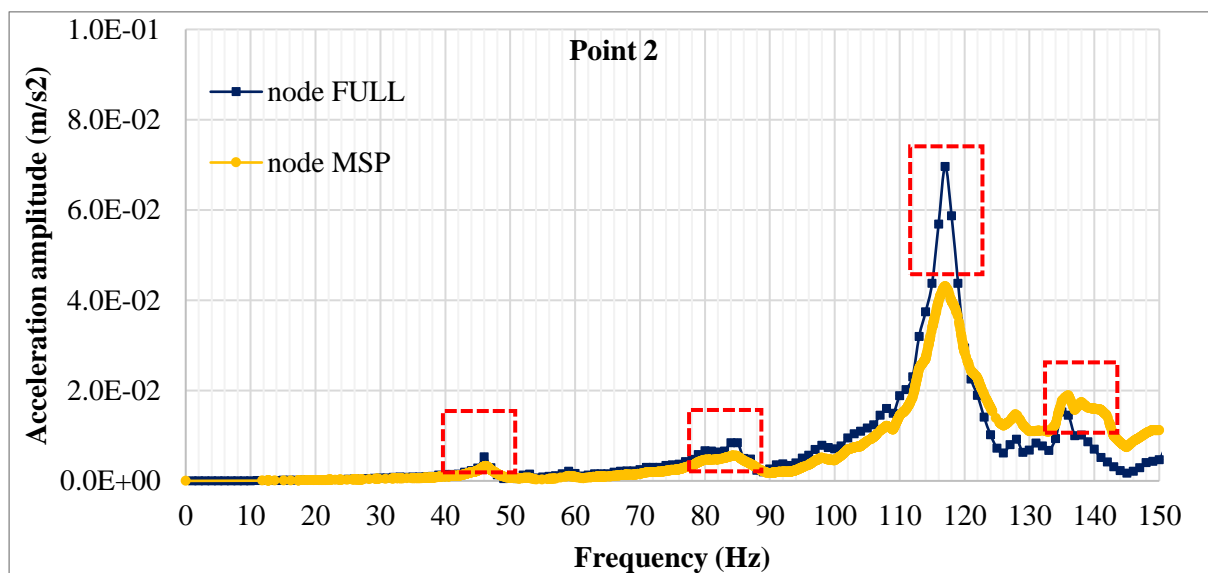


Figure 4.4. Harmonic response Ansys Workbench in Point 2

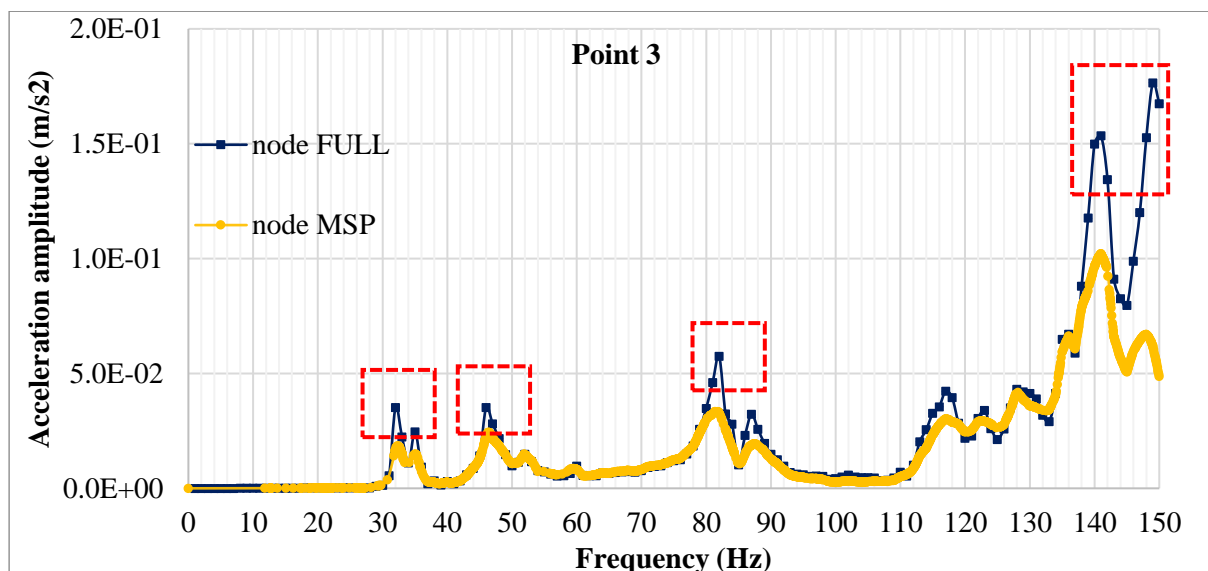


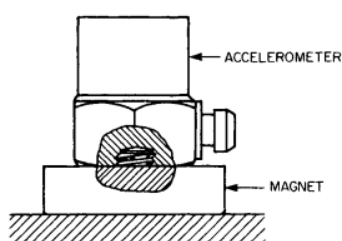
Figure 4.5. Harmonic response Ansys Workbench in Point 3

In all the points, both methods present the same shape, but the Full method generally has a higher response than the MSP, this behavior is expected since the full harmonic analysis (direct method) permit the exact solution by solving the system of equations and the MSP method approximates the solution and its accuracy depends on whether an adequate number of modes have been extracted.

5. MEASUREMENTS

5.1.Measurement system description

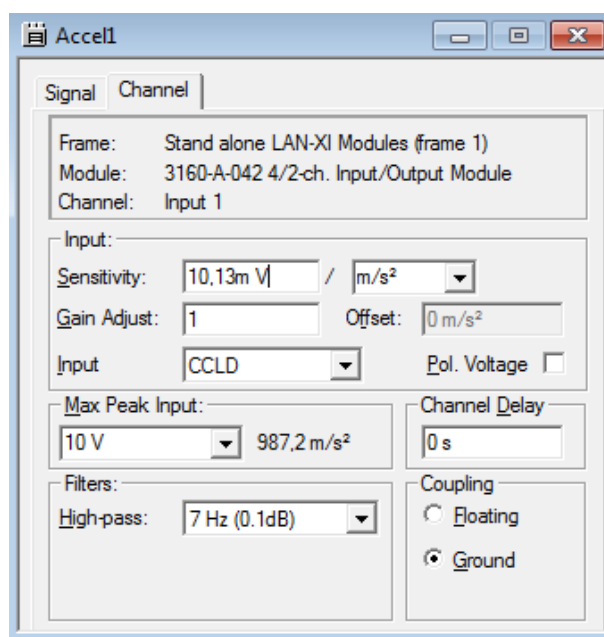
For modal response measurements, on deck 14 and deck 15 the acceleration was measured only in the vertical direction with the Brüel and Kjær transducer type 4526, the sensitivity is 10 mV/m/s², Figure 5.1. The frequency range was from 0 to 50 Hz for decks and 0 to 150 Hz for cabins. The transducers were mounted by attaching to the deck surface using a permanent magnet.



a. Mounting type



c. Accelerometer B&K4526

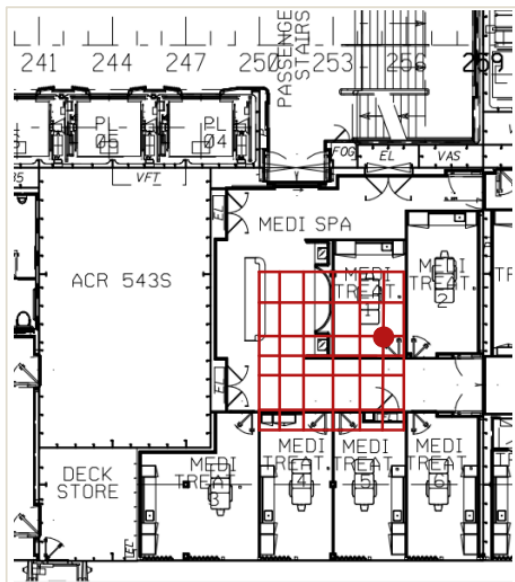


b. Settings for measurement

Figure 5.1. Transducer characteristics

5.2.Deck 14

For deck 14, a grid of 5.12 x 5.43 m was arranged with six divisions in each direction to perform the measurements, Figure 5.2, between frames 250 and 256 in the x-direction and between 7.985 and 13.415 m in the y-direction. The accelerometer was located on the position of the red circle and the deck was perturbed by hammering at each point in the other intersections of the grid, it should be remarked that the grid coincides with the stiffener's arrangements, then, the hammering was made over the stiffeners.



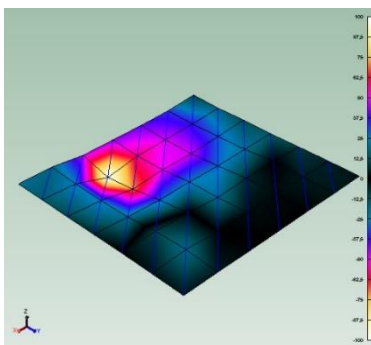
a. Grid prepared for deck 14
measurements



b. Hammering on the grid points

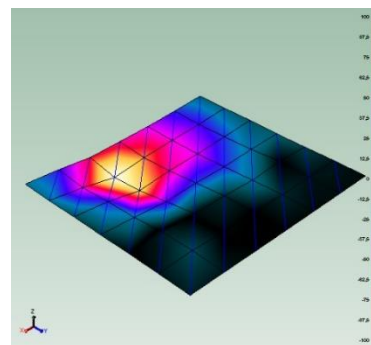
Figure 5.2. Measurements on deck 14

The signal was acquired and processed with Brüel and Kjær software BK Connect and the results of the first eight modes are in Figure 5.3.



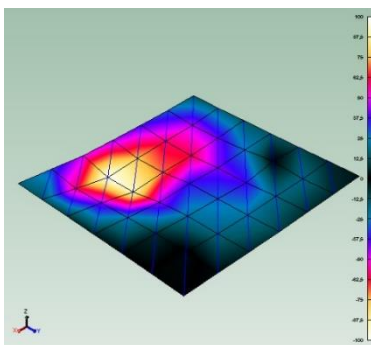
a. Mode 1, 20.65 Hz

Damping 1.850 %, Complexity 0.174



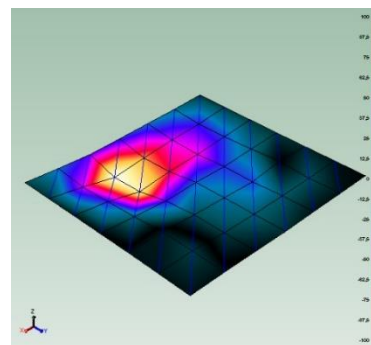
b. Mode 2, 23.22 Hz

Damping 1.846%, Complexity 0.049



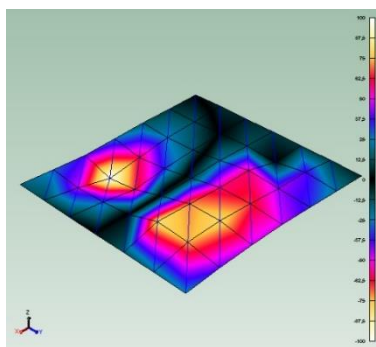
c. Mode 3, 24.71 Hz

Damping 5.361 %, Complexity 0.084



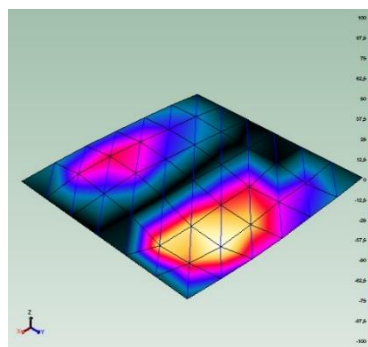
d. Mode 4, 25.21 Hz

Damping 2.115 %, Complexity 0.067



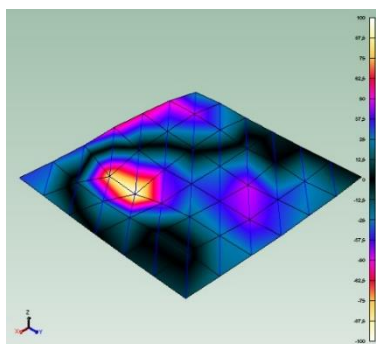
e. Mode 5, 27.67 Hz

Damping 2.004 %, Complexity 0.436



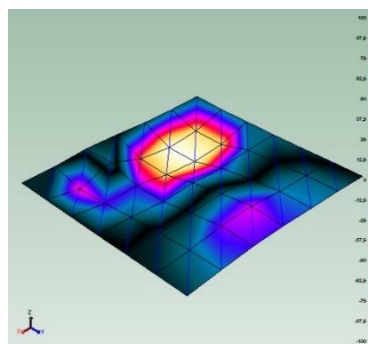
f. Mode 6, 29.83 Hz

Damping 2.704 %, Complexity 0.245



g. Mode 7, 33.82 Hz

Damping 1.762 %, Complexity 0.749



h. Mode 8, 36.61 Hz

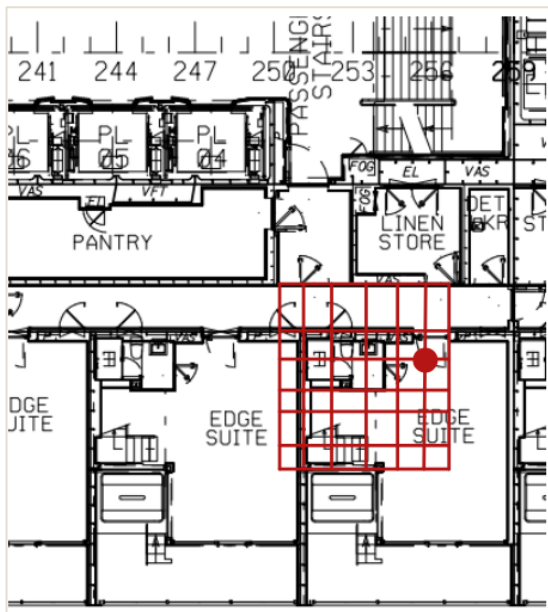
Damping 2.626 %, Complexity 0.665

Figure 5.3. Results of modal measurements on deck 14

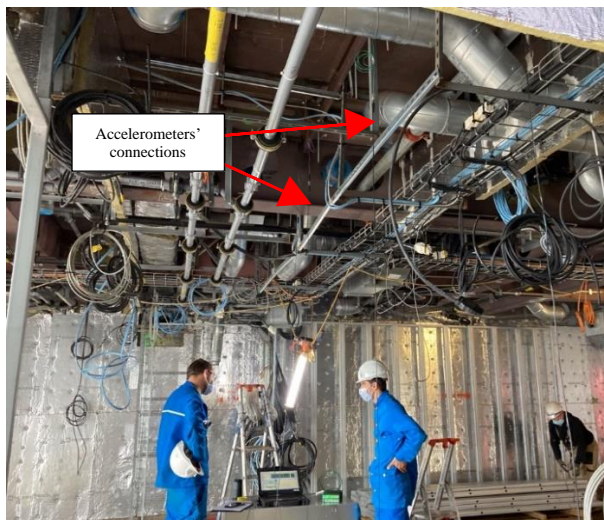
5.3.Deck 15

For deck 15, we followed a similar grid like the one used in deck 14 with six divisions in each direction to perform the measurements, Figure 5.4, between frames 250 and 256 in the x-direction and between 7.985 and 13.535 m in the y-direction. Contrary to deck 14, for this case, we made seven measurements with seven accelerometers at each line of the grid below the deck and the deck was perturbed by hammering in the red point.

In this case, the grid was a bit modified since the accelerometers were not located exactly at the stiffener's positions but the nearest possible due to various elements as cables and pipes that were already installed under deck 15. The test was made below the deck because the floating floor also was installed at the time of the measurements.

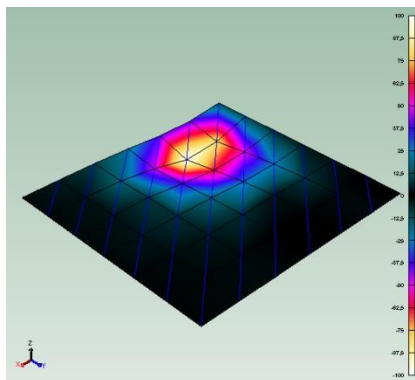


a. Grid prepared for deck 15 measurements



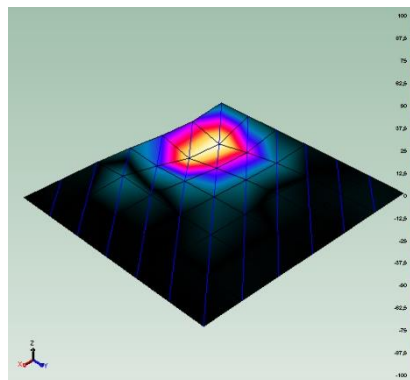
b. Position of accelerometers below deck 15

Figure 5.4. Measurements on deck 15



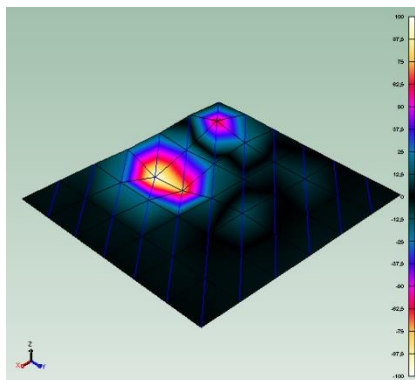
a. Mode 1, 28.31 Hz

Damping 0.981 %, Complexity 0.193



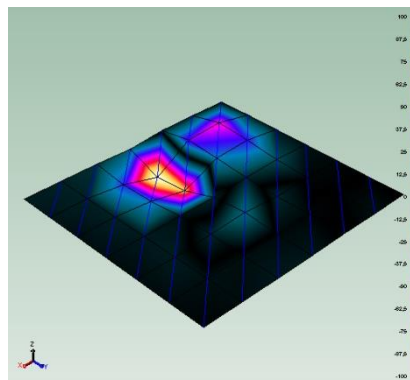
b. Mode 2, 30.09 Hz

Damping 0.644 %, Complexity 0.080



c. Mode 3, 34.46 Hz

Damping 0.766 %, Complexity 0.464



d. Mode 4, 36.08 Hz

Damping 0.484 %, Complexity 0.562

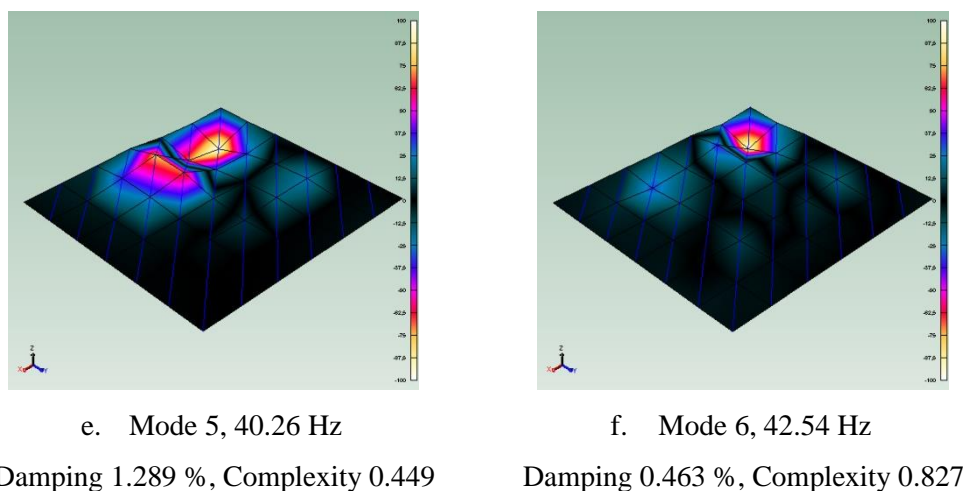


Figure 5.5. Results of modal measurements on deck 15 with floating floor

5.4.Cabin “RAMSESS”

Measurements were made in cabin “Ramsess” at girder 1 and girder 2 marked on Figure 5.6 by separate by perturbing the structure with a small hammer. Eleven accelerometers were placed at the first girder, and then at the second girder.

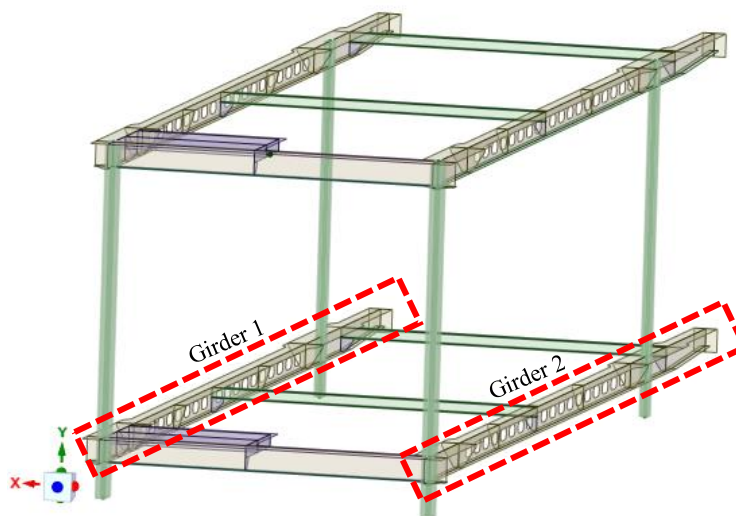
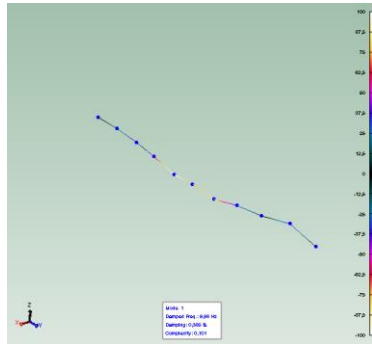


Figure 5.6. Zones of measurement for “Ramsess” cabin

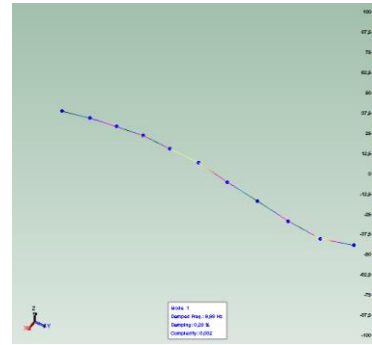
The modal results are presented in Figure 5.7, it should be remarked that the coordinate systems are different for the model and the modal results. The z -direction in the measurements is parallel to the x -direction and the model, and the x -direction in the measurements is parallel to the y -direction and the model. The main displacement in modes 1, 2, and 3 is on z -direction (x -direction in the model), in modes 4, 5, and 6 the main displacement is on x -direction (y -direction in the model).

Girder 1

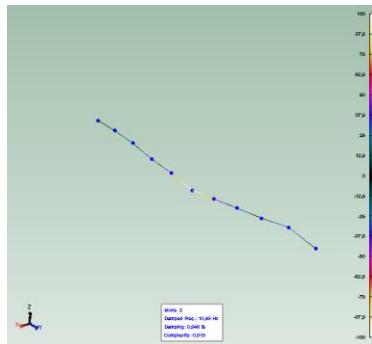


a. Mode 1, 9.98 Hz

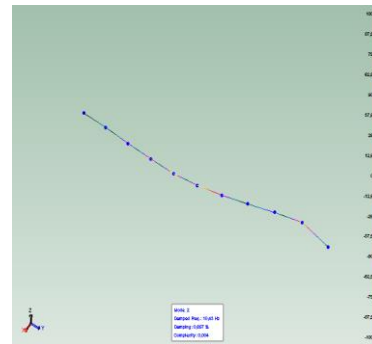
Girder 2



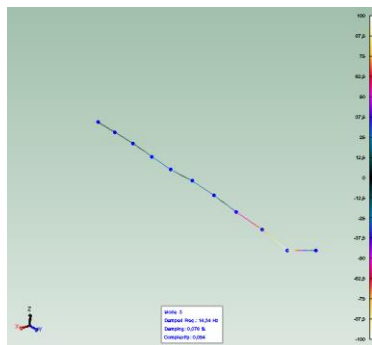
b. Mode 1, 9.98 Hz



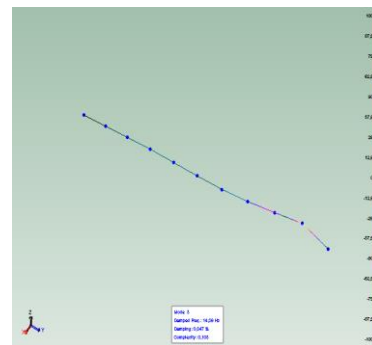
c. Mode 2, 10.46 Hz



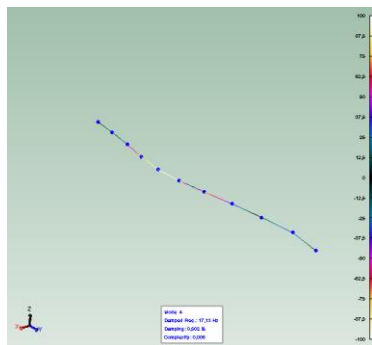
d. Mode 2, 10.43 Hz



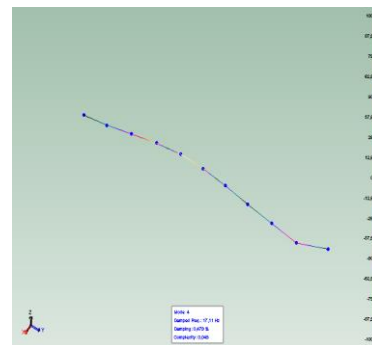
e. Mode 3, 14.34 Hz



f. Mode 3, 14.39 Hz



g. Mode 4, 17.13 Hz



h. Mode 4, 17.11 Hz

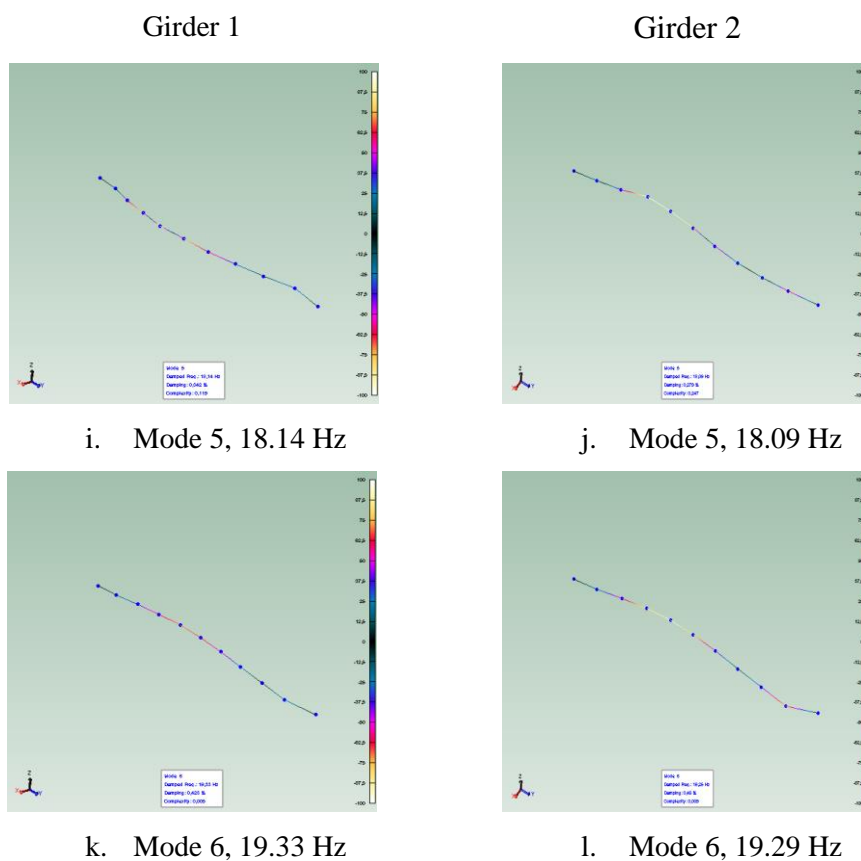
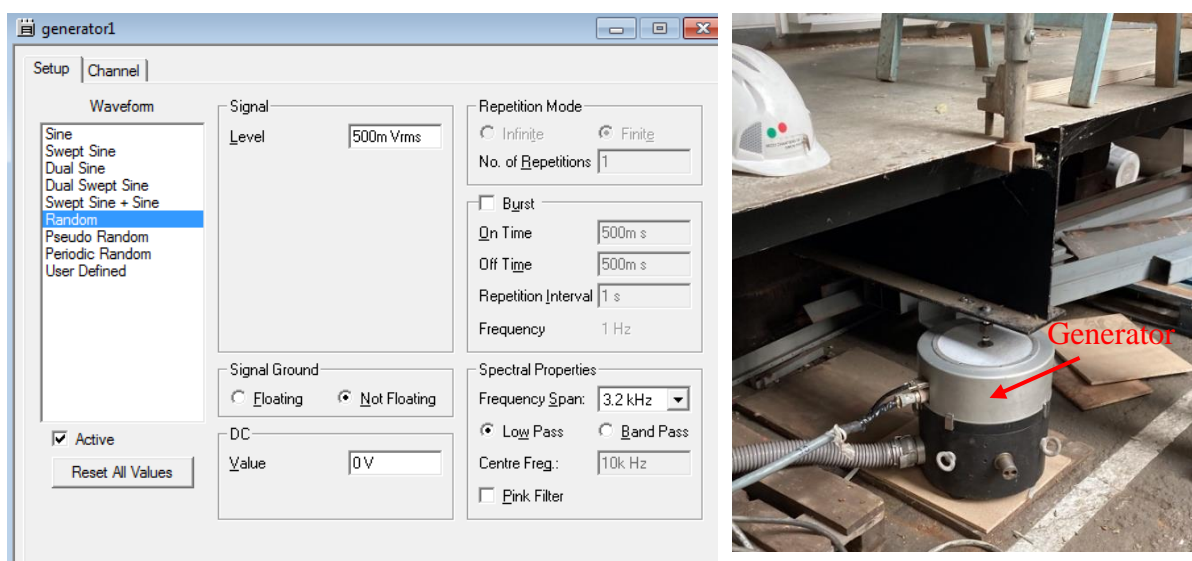


Figure 5.7. Modal results from measurements on cabin “Ramsess”

5.5. Cabin model

This is the only structure where harmonic response measurements were performed, the excitation force was generated by a shaker with the settings of Figure 5.8 a.



a. Generator settings

b. Generator installed on the cabin

Figure 5.8. Generator used to generate external excitation

The signal recorded for the response was acceleration, the analysis of the response was made with Pulse™ Labshop software version 22.2.0.303 and FFT spectrum averaging. Two accelerometers were located at each measurement area, Figure 4.2 obtaining the results in Figure 5.9.

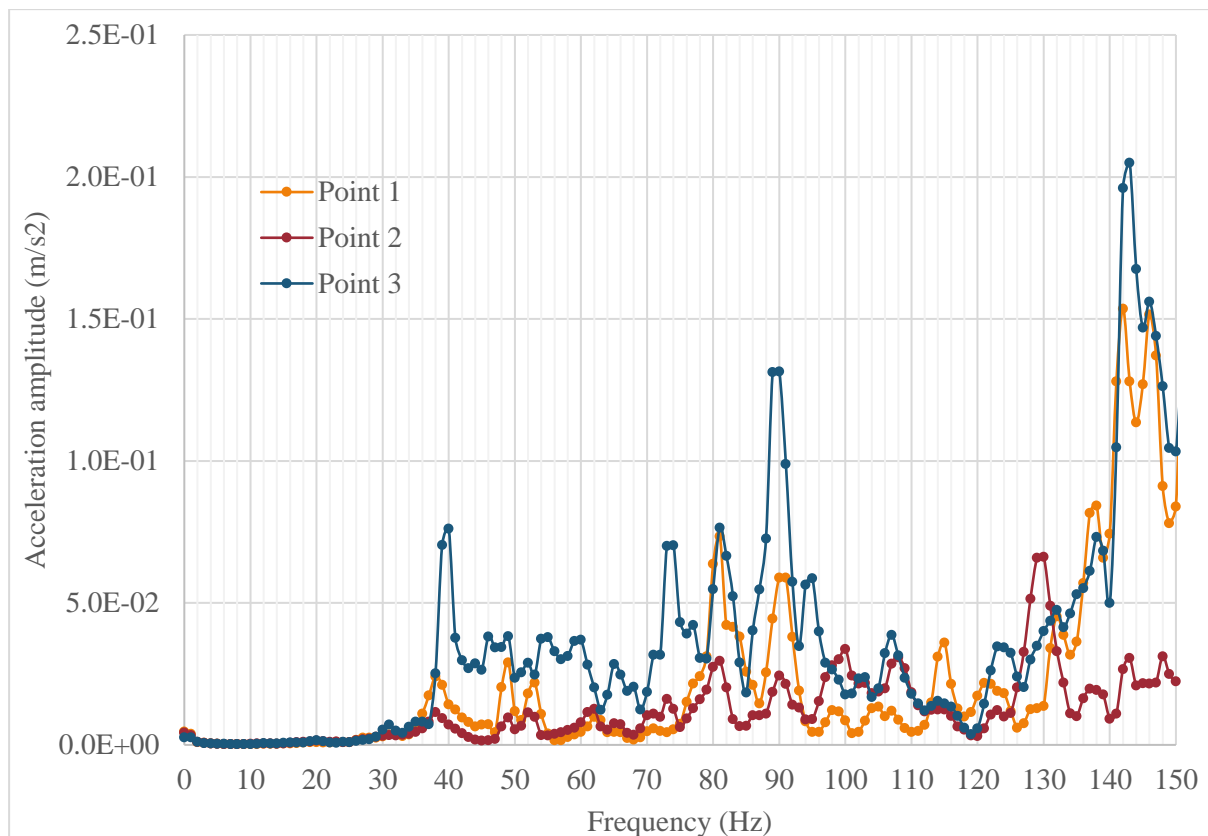


Figure 5.9. Measurement results on three areas of the cabin model balcony

In points 1 and 3 the two accelerometers were located one next to the other but in point 2, they were located separately as shown in Figure 5.10.



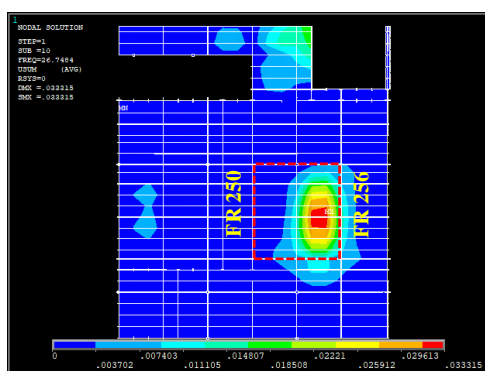
Figure 5.10. Measurement on Point 2

6. CORRELATION

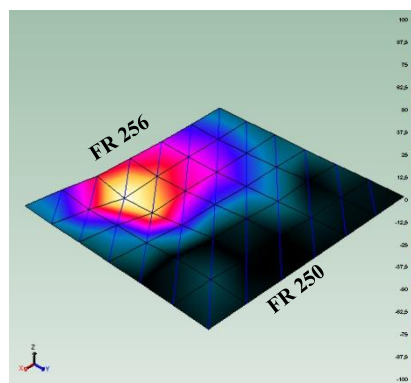
6.1. Modal analysis in decks

The validation of the modal measurements is made by visual verification and comparison with shape extracted from the finite element models. As visually there are some modes with similar shapes in the measurements, the modes selected to compare with finite element results are the ones with the lowest complexity considering that the finite element solution was made excluding the complex term.

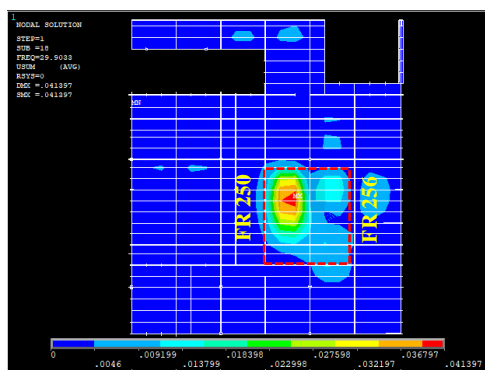
The results of measurements on deck 14 show that the first four modes seem to have the same shape as mode 1 from finite element results in Ansys Classic and Ansys Workbench, as modes 5 and 6 in the measurement with mode 2 in finite element results, Figure 6.1.



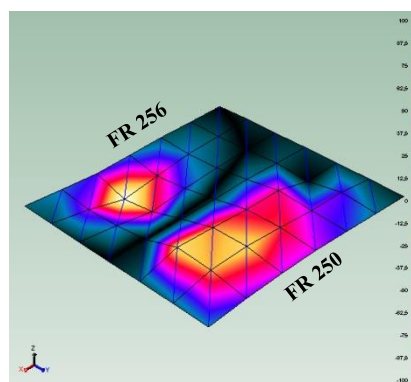
a) Ansys Classic, 26.8 Hz



b) Measurements, 23.2 Hz



c) Ansys Classic, 29.9 Hz



d) Measurements, 27.7 Hz

Figure 6.1. Shape mode from finite element and measurements on site for deck 14

Table 6.1. Comparison of results between finite element and test results for deck 14

	Mode 1 (23.2 Hz)		Mode 2 (27.7 Hz)	
	Hz	% Difference with test	Hz	% Difference with test
A. Classic	26.7	15.2 %	29.9	8.1 %
WB 0.50	25.1	8.0%	26.7	3.5%
WB 0.60	25.2	8.6%	27.0	2.5%
WB 0.75	26.0	11.9%	28.2	1.8%
WB 0.80	26.0	11.9%	28.2	1.8%
WB 0.90	26.7	15.2%	29.5	6.6%

For this structure, it was possible to apply the AutoMAC criterion which is a variation of the Modal Assurance Criterion (MAC), Eq. 6.1, for only one set of mode shapes coming from the test results. Regular MAC is calculated as the normalized scalar product of two sets of vectors $\{\varphi_A\}$ and $\{\varphi_X\}$ which are the analytical and test modal vectors.

$$MAC(r, q) = \frac{|\{\varphi_A\}_r^T \{\varphi_X\}_q|^2}{(\{\varphi_A\}_r^T \{\varphi_A\}_r) (\{\varphi_X\}_q^T \{\varphi_X\}_q)} \quad \text{Eq. 6.1}$$

The calculation assigns a value of 1.0 to test and analyze mode shape pairs that exactly match. A value of 0 is given to those pairs that are completely independent or unrelated and can indicate a problem (Pastor, Binda, & Harcarik, 2012).

The matrix in Figure 6.2 confirms that the first mode appears between 20 and 25 Hz, the second mode is between 27 and 30 Hz, and the third mode is not clearly defined.

	20,648	23,224	24,714	25,208	27,670	29,830	33,817	36,611	41,120	41,599	45,148
20,648	1,000	0,915	0,878	0,877	0,351	0,216	0,045	0,336	0,045	0,072	0,005
23,224	0,915	1,000	0,894	0,901	0,279	0,179	0,044	0,330	0,039	0,069	0,014
24,714	0,878	0,894	1,000	0,964	0,221	0,095	0,111	0,392	0,074	0,090	0,012
25,208	0,877	0,901	0,964	1,000	0,241	0,135	0,179	0,455	0,087	0,106	0,018
27,670	0,351	0,279	0,221	0,241	1,000	0,926	0,138	0,302	0,142	0,156	0,100
29,830	0,216	0,179	0,095	0,135	0,926	1,000	0,248	0,320	0,116	0,126	0,102
33,817	0,045	0,044	0,111	0,179	0,138	0,248	1,000	0,586	0,392	0,269	0,095
36,611	0,336	0,330	0,392	0,455	0,302	0,320	0,586	1,000	0,471	0,394	0,091
41,120	0,045	0,039	0,074	0,087	0,142	0,116	0,392	0,471	1,000	0,934	0,380
41,599	0,072	0,069	0,090	0,106	0,156	0,126	0,269	0,394	0,934	1,000	0,492
45,148	0,005	0,014	0,012	0,018	0,100	0,102	0,095	0,091	0,380	0,492	1,000

Figure 6.2. AutoMAC matrix for modes on deck 14

The results of measurements on deck 15 with a floating floor show that the first two modes seem to have the same shape as mode 1 in finite element results for Ansys Classic and Ansys Workbench, modes 3 and 4 in the measurement seem to have the same shape as the mode 2 in finite element results. It should be noticed that for first and second mode of deck 14 and first mode of deck 15, the range of frequency of all the results is small but the same behaviour does not appear for second mode of deck 15, then this last result could not be trustable.

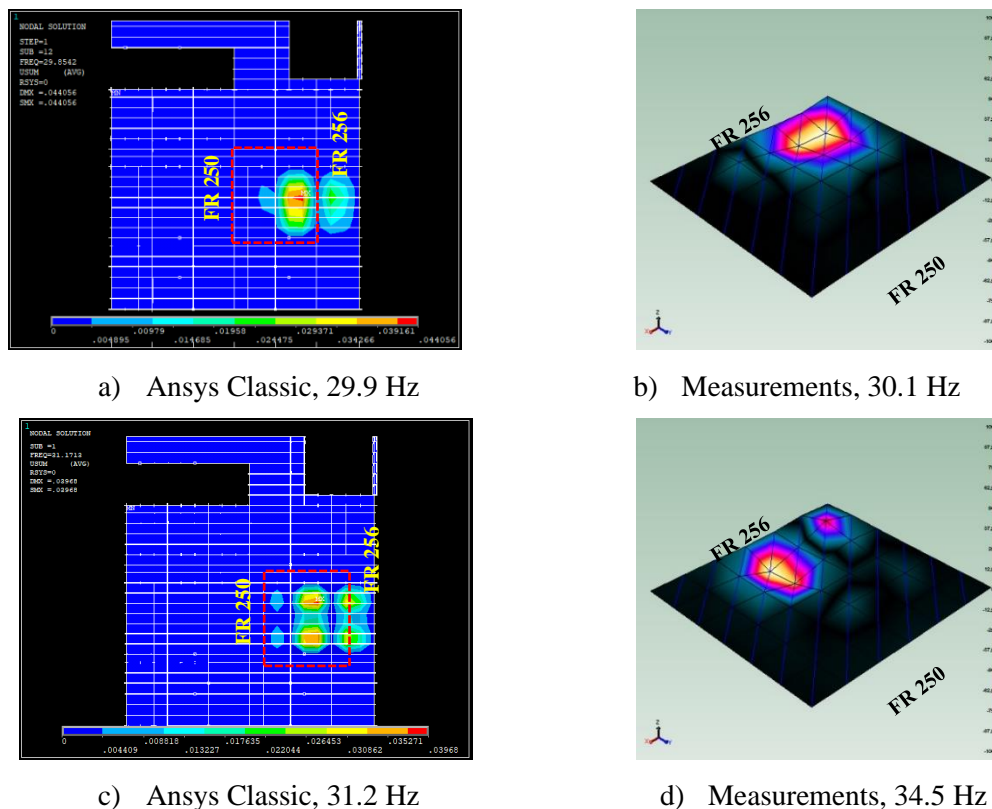


Figure 6.3. Shape mode from finite element and measurements on site for deck 15

Table 6.2. Comparison of results between finite element and test results for deck 15

	Mode 1 (30.1 Hz)		Mode 2 (34.5 Hz)	
	Hz	% Difference with test	Hz	% Difference with test
A. Classic	29.9	0.8 %	31.2	9.5 %
WB 0.50	32.4	7.6%	41.4	20.1%
WB 0.60	33.5	11.5%	43.5	26.4%
WB 0.75	35.5	18.1%	45.5	32.0%
WB 0.80	36.4	21.1%	46.5	34.9%
WB 0.90	36.4	21.1%	46.5	34.9%

6.2. Modal analysis in cabin “RAMSESS”

The results of measurements on “Ramsess” cabin model show a good definition of the modes’ shape behaving as a beam as shown in Figure 6.4. For the first result, where the beams move in the x-direction, the fixed support shows a better correlation than simply supported support.

On contrary, for the second and third modes where the beams move in the y-direction, simply supported condition shows a better correlation, Table 6.3. For comparison of test results, an average between the girders is used.

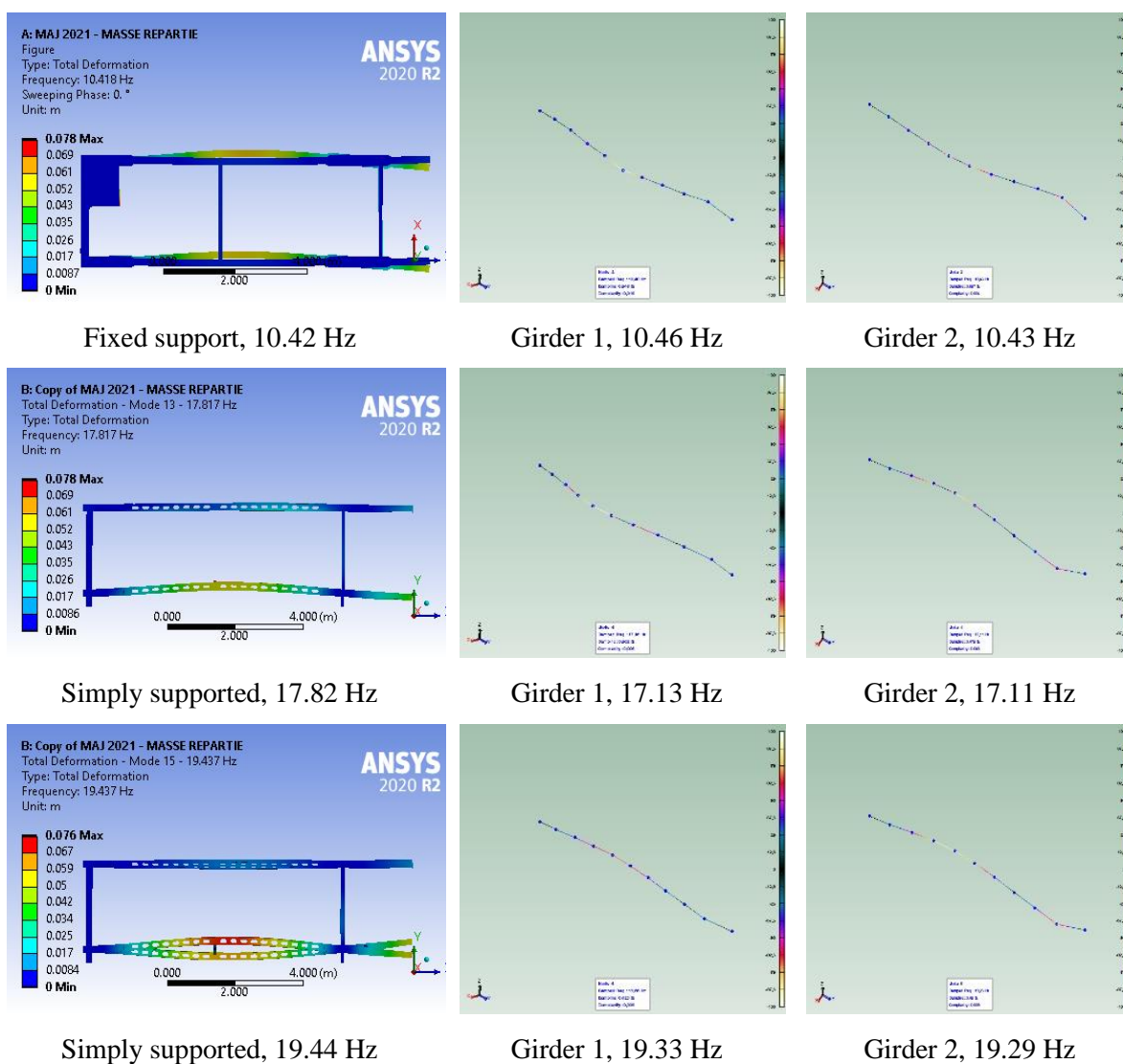


Figure 6.4. Shape mode from finite element and measurements on site for cabin “RAMSESS”

Table 6.3. Comparison of results between finite element and test results for “Ramsess” cabin

	Mode 1 (10.5 Hz)		Mode 2 (17.1 Hz)		Mode 3 (19.3 Hz)	
	Hz	% Difference with measurements	Hz	% Difference with measurements	Hz	% Difference with measurements
Simply Supported	10.20	2.35%	17.82	4.09%	19.44	0.67%
Fixed	10.42	0.24%	18.07	5.55%	19.76	2.33%

6.3. Harmonic analysis in cabin model

The average amplitude of the harmonic response in Point 1 correlates quite well in some points only, as shown in Figure 6.5; for this work I establish that a good correlation exists when the difference in frequency and amplitude of the peaks is less than 10%. The first peak of the simulation appears at 32 Hz and there is not a similar response in the measurements, the second peak has a good correlation and appears at 35 Hz for the simulation and 38 Hz for the measurements with a difference of 8% in the frequency and equal amplitude. The third, fourth and fifth peaks has medium good correlation, 6%, 2% and 1% difference for the frequency but 33%, 50% and 17% difference for amplitude.

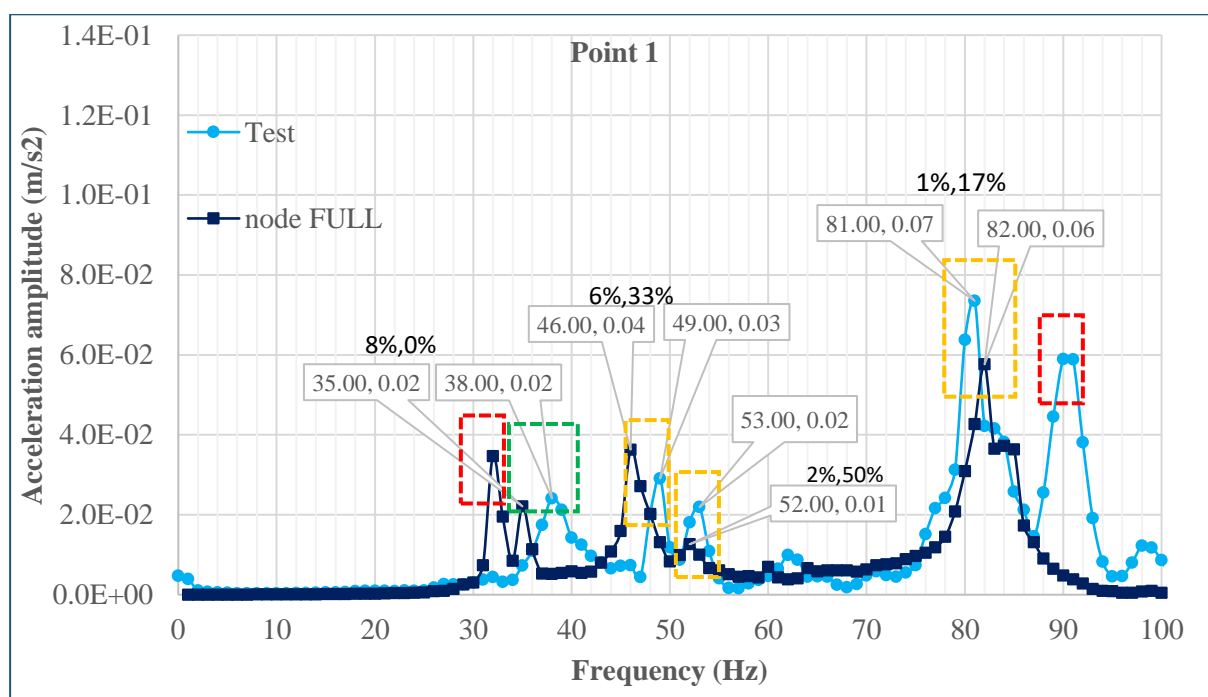


Figure 6.5. Harmonic response comparison for Point 1 (0-100 Hz)

These gaps could be generated from the uncertainty of the finite element model, the level of details of the model, and the additional uncertainty coming from the structure's construction process which is not considered in the model. The high response at 90 Hz in the measurements may be originated by a resonance in the connection between the generator and the cabin.

In Point 2, Figure 6.6, the amplitude does not correlate quite well. It should be remarked that Point 2 results are the average of two points located over the central girder and near to one of the supports (Figure 3.8 a.), the differences in amplitude could come from a bad representation of the support condition. In the model prepared for the simulation, the condition is simply supported restricting any vertical displacement, but the prototype just lay down over wood's pieces, as shown in Figure 6.7.

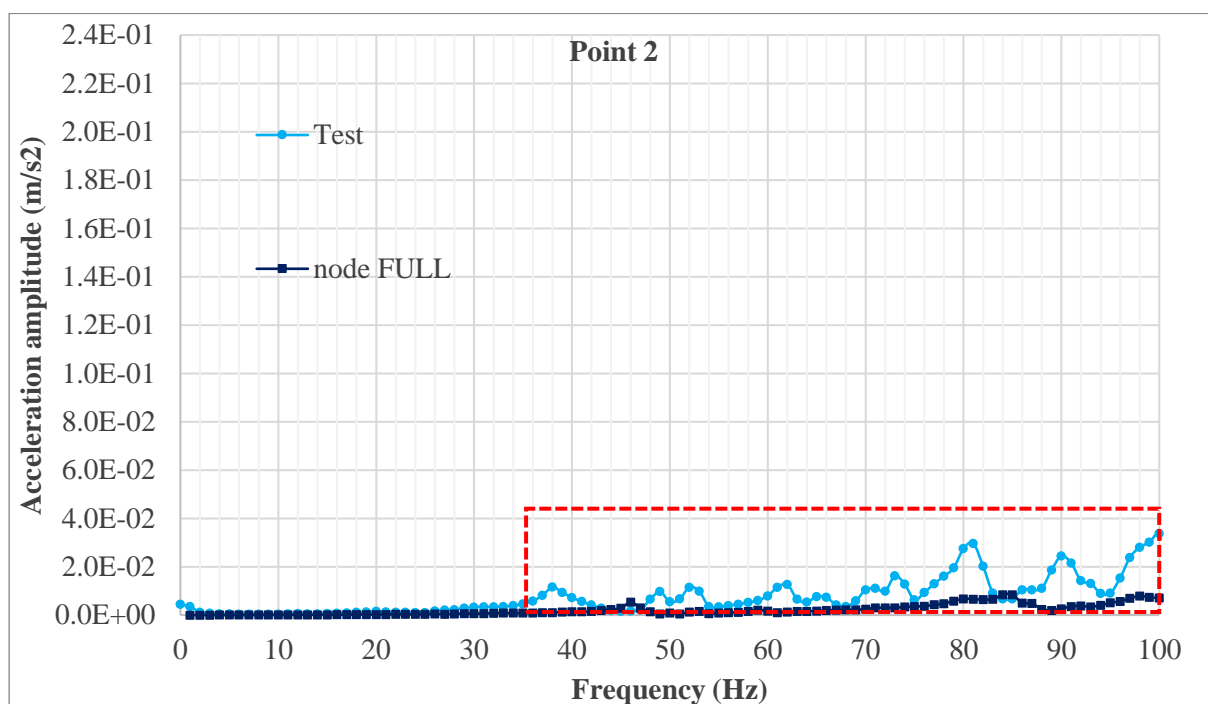


Figure 6.6. Harmonic response comparison for Point 2 (0-100 Hz)

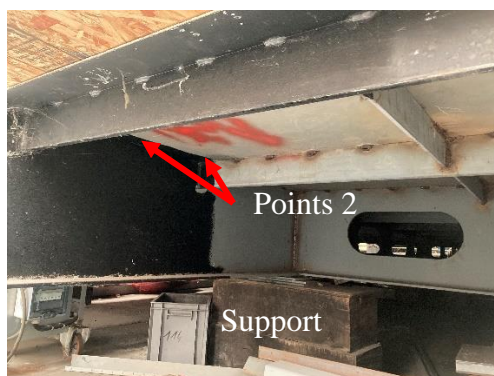


Figure 6.7. Support of the cabin prototype

The correlation in the third point is not quite good neither in terms of amplitude nor in frequency between 30 and 100 Hz as shown in Figure 6.8. Like Point 1, the high response at 90 Hz in the measurements may be originated by a resonance in the connection between the generator and the cabin.

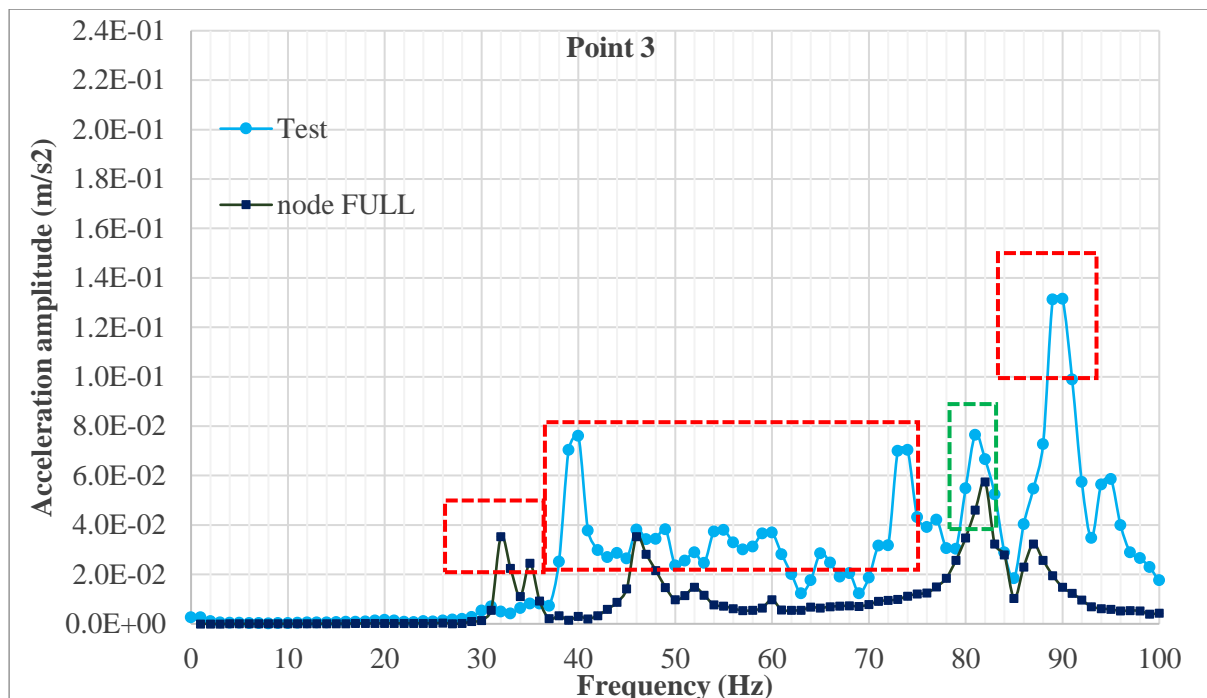


Figure 6.8. Harmonic response comparison for Point 3

The response of Point 3 in the simulation is similar to the response in Point 1, this makes sense since these points are in symmetry. We would expect the same similarity in the test response, but the difference is clear in Figure 5.9 where the three measurements are in the same graph. I would say that especially in this part, the model is not a good representation of the reality since in this area are additional elements as pipes attached to the structure that could be affecting the response, Figure 6.9.

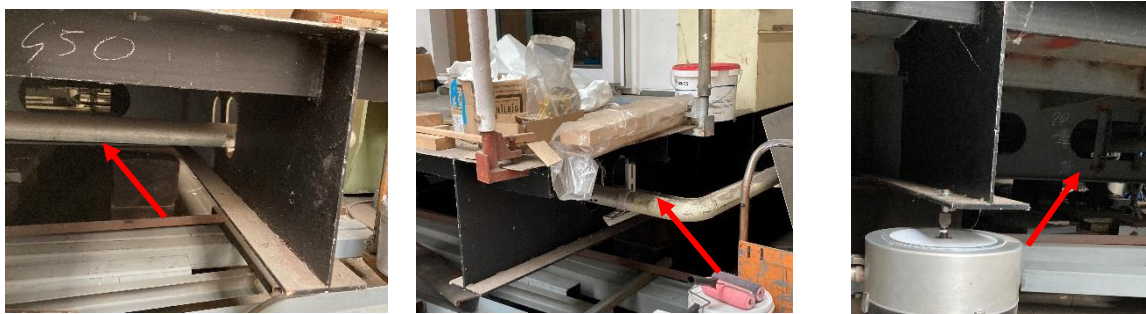


Figure 6.9. Close up to the area under Point 3

7. CONCLUSIONS AND PERSPECTIVE

It was not possible to find a consistent relation between all the results of the modal analysis made in Ansys Classic and Ansys Workbench. Except for a few modes, the shapes are not always coincident, and the differences increase for higher modes. It would be ambitious to try to find the exact source of differences, but it appears to start from the fact that the models are not equal, each application uses different types of elements, and they are not distributed in the same manner on the decks. Even if the method for solving the eigenvalue problem is the same, the initiation of the iterative process could also lead to differences in the response. Based on the results of this work, the use of the simplified method developed by the company with APDL macros in Ansys Classic to do the modal analysis is currently the best option, but it has the drawback that is not currently adaptable to complex forms as curve surfaces, changes in thickness or girders size. However, if an upgrade is desired it is a good opportunity to migrate those macros to a 3D modelling software compatible with Ansys Workbench, for example, Space Claim which allows the modelling by scripts.

It should be mentioned that the company has already performed this kind of comparison between models in Workbench and Ansys Classic, trying different mesh sizes and types of elements for both applications. Their conclusions are consistent with the conclusions based in this work about Classic vs. Workbench.

The correlation of the measurement with the finite element method is quite good for deck 14, it is not happening the same for deck 15, some parameters could be influencing the resultant frequencies and has not been considered in the models, as residual stresses, distortions, additional weights due to welding, a non-accurate estimation of the surface mass existent during the test, the error of the measurement equipment and some perturbations during the test due to other works because the ship is under construction. Especially for deck 15, where the floating floor has already been installed, the energy transmitted through the hammer could not be sufficient to properly generate and capture the modal response. Then, considering all these non-ponderable sources we can expect, as best, an approximation to a range of frequencies to avoid.

Contrary to the other structures, the results for cabin “Ramsess” show a good correlation between the finite element model and the measurements for modal analysis, the maximum difference between the natural frequencies was 5% even with different kinds of supports. As the structure is formed mainly by beams, the response was as expected for a typical beam behaviour, then, the mode shapes were easy to identify and correspond almost exactly with the

shape registered on the measurements. This is confirmation that the accuracy of the model gets lost as the structure becomes more complex and it is a good practice to test the structure at different stages of construction to verify the weak points of a finite element model and how to improve it.

The correlation of the harmonic response on the cabin model is good in terms of amplitude and the small differences in peak frequencies could be explained due to the uncertainty of the finite element model. The level of details of the model is moderate, it includes the steel structure, carpet, insulation, and an additional 1-ton weight located in the upper deck during the test, but it excludes non-structural parts like doors and smaller weights. There is always additional uncertainty coming from the structure's construction process which is not considered in the model.

The other two points do not correlate quite well, in the second point, this happens especially at low frequencies probably due to an inaccurate representation of the supports. The simply supported condition imposed in the model restricts any vertical displacement and the prototype just lays down over a base and could be moving upwards. The third point bad correlation could happen because some elements as pipes are attached to the structure in this area and they are not included in the model. The big amplitude in points 1 and 3 at 90 Hz in the test results could be coming from resonance in the connection's piece of the shaker that should be investigated. The differences at high frequencies could also be explained by the low effectiveness of the finite element model at high frequencies due to high modal density, it would be a good opportunity to probe the application of statistical energy analysis (SEA).

8. REFERENCES

- Asmussen, I., Menzel, W., & Mumm, H. (2001). *Ship Vibration. GL-Technology*. Hamburg: Germanischer Lloyd.
- Chen, C. J., Liu, W., & Chern, S. M. (1994). *Vibration Analysis of Stiffened Plates*. Chung Cheng Institute of Technology, Department of Civil Engineering. Taiwan: Elsevier Science. Ltd.
- Coppolino, R. N. (2010). Finite Element Methods of Analysis. In A. G. Piersol, & T. L. Paez, *Harris' Shock and Vibration Handbook* (Sixth ed.). McGraw-Hill.
- Ferrari, A., & Rizzuto, E. (2001). *Experimental Modal Analysis of a Ship Deck Structure*. DINAV-Department of Naval Architecture & Marine Technologies. Genoa: University of Genoa.
- Gérardin, M., & J.Rixen, D. (2015). *Mechanical Vibrations, Theory and Application to Structural Dynamics* (Third ed.). Chichester, West Sussex, United Kingdom: John Wiley & Sons, Ltd.
- Le Sourne, H. (2017, May). Ship Vibrations. *EMSHIP master class notes*. ECN.
- Leissa, A. W. (1969). *Vibration of plates*. Washington, D.C. : National Aeronautics and Space Administration .
- Pastor, M., Binda, M., & Harcarik, T. (2012). Modal Assurance Criterion. *Procedia Engineering*, 543-548.
- Warburton, G. (1954). The Vibration of Rectangular Plates. *Proceedings of the Institution of Mechanical Engineers*, 371-384.